



## Preserving our heritage: A photogrammetry-based digital twin framework for monitoring deteriorations of historic structures

Xiangxiong Kong<sup>a,\*</sup>, Ronny Garrett Hucks<sup>b</sup>

<sup>a</sup> Department of Physics and Engineering Science, Coastal Carolina University, Conway, SC 29528-6054, United States of America

<sup>b</sup> Formerly Department of Physics and Engineering Science, Coastal Carolina University, Conway, SC 29528-6054, United States of America



### ARTICLE INFO

**Keywords:**

Digital twin  
Cultural heritage  
Structural health monitoring  
Historic structures  
Crack  
Photogrammetry  
Computer vision

### ABSTRACT

Preservation of historic structures is a global challenge for governments and site owners, as accumulated deteriorations could weaken the structural integrity. Recent advances in the digital twin in civil and infrastructure engineering have shown great promise in creating virtual models of a physical entity under time-varying physical states. Because of this unique feature, assessing time-varying structural deteriorations become feasible. This paper presents a novel methodological attempt of health monitoring for historic structures by integrating photogrammetry technologies and point cloud processing algorithms into a digital twin framework. To make this viable, virtual models of the physical structure at different inspection times are first created via photogrammetry technologies. Then, a bridge health monitoring method is established to align two virtual models together and further differentiate the changes provoked by structural deterioration. We validate the proposed methodology in a historic stone arch bridge for detecting multiple simulated structural deteriorations.

### 1. Introduction

Preservation of historic sites is a global challenge for government agencies and site owners. Due to long service times and natural impacts caused by rainfall, flooding, sunlight, humidity, earthquake, and/or strong wind, many historic sites are prone to structural deterioration. This becomes particularly critical for historic structures such as bridges, buildings, arenas, towers, and fortifications, as accumulated deteriorations could weaken the structural integrity and cause catastrophic failures. Furthermore, the safety of historic structures could be threatened by man-made disasters such as military combat (e.g., recently reported in Syria [1], Iraq [2], Afghanistan [3], and Ukraine [4]). Therefore, affordable and flexible methodologies are urgently needed to assess the deterioration of historic structures and cultural heritage sites.

Traditionally, human inspection is the most common approach for evaluating the structural safety of historic structures [5], through which structural damage such as cracks, concrete spalling, and excessive deformations can be observed. However, due to the complexity of the structural characteristics, human inspection is usually time-consuming and requires trained technicians or licensed engineers, which brings an extra cost to the owners of historic structures. Hence, performing inspections on a routine basis may not be easily achievable.

To address the above concern, researchers [6] adopted advanced technologies to evaluate the condition of historic structures by deploying physical sensors. Such sensing technologies vary depending on the characteristics of the measurements to be investigated. For instance, environmental sensors can measure wind speed and air pressure [7]; vibration sensors can record accelerations and displacements [8–10]; and load pressure cells can collect pressure measurements in structural elements [11]. Despite the successes of these methods, they usually require extensive efforts to install sensors, cables, and data acquisition systems. Also, once deployed, the monitoring system may not be easily transferred to different historic sites. Therefore, only prioritized sites can benefit from such technologies.

In this paper, we propose a novel health monitoring methodology for historic structures using a digital twin framework. To make this viable, we build virtual models of the physical entity of the historic structure at different inspection times via photogrammetry technologies. Then, a bridge health monitoring method is established to align two virtual models together and further differentiate the changes provoked by the structural deterioration. We validate the proposed methodology in a historic stone arch bridge and assess the viability of our method in detecting multiple simulated structural deteriorations. The remainder of the paper is structured as follows: Section 2 reviews the related work in

\* Corresponding author.

E-mail addresses: [xkong@coastal.edu](mailto:xkong@coastal.edu), [kuxkong@gmail.com](mailto:kuxkong@gmail.com) (X. Kong).

computer vision-based methods, photogrammetry-based methods, and digital twin in the context of cultural heritage preservation; [Section 3](#) identifies the research gap and clarifies our contributions; [Section 4](#) illustrates the proposed research methodology and explains technical details; [Section 5](#) reports the study site and shows the results of experimental validations; [Section 6](#) demonstrates additional investigation results of the proposed method against simulated structural deterioration; [Section 7](#) discusses the viability, adaptability, and limitations of our proposed method; and [Section 8](#) concludes the paper.

## 2. Related work

### 2.1. Computer vision-based SHM in cultural heritage

Computer vision technologies have brought increasing attention to the Structural Health Monitoring (SHM) of historic structures for being able to offer non-contact and low-cost solutions. Utilizing consumer-grade digital cameras including the onboard cameras from Unmanned Aerial Vehicles (UAVs), images/videos can be collected in the field and processed by computer vision algorithms. As a result, image features related to different types of structural damage can be detected, extracted, and quantified.

In general, vision-based approaches for inspecting historic structures can be categorized as machine learning-based methods and non-learning-based methods. Through training a classifier *via* pre-labeled image patches, the machine learning algorithm can automatically identify the structural damage from new images taken under a similar environment. Machine learning-based methods are effective when the damage features are too subtle to be visually identified and/or contaminated by other irrelevant image features. Therefore, machine learning-based methods have been used in many evaluations of historic structures. Zou *et al.* [12] developed a vision-based method for identifying the missing structural components in a historic building through image processing and deep learning. A deep learning-based method for inspecting the spalling in historic masonry structures was proposed by Wang *et al.* [13]. A faster Region-based Convolutional Neural Network (R-CNN) method for identifying three structural damage types (*i.e.*, spalling, exposed bricks, and cracks) in heritage structures was developed by Mansuri and Patel [14], significantly reducing inspection errors, time, and cost. Pathak *et al.* [15] trained a convolution neural network to classify spalling and cracks from an image dataset of a historic temple in Thailand. Haturi *et al.* [16] leveraged R-CNN to detect multiple types of stone deteriorations and further mapped them back to orthophotos. For a comprehensive review of recent advances in machine learning-based methods in SHM of historic structures, the readers are referred to [17].

Non-learning-based methods, on the other hand, can directly extract damage-induced features from digital images and/or videos without training the classifiers. For instance, cracks can be directly identified by finding the edge-like features [18], applying image correlation [19], performing image segmentation [20], and quantifying crack breathing behavior [21]; a loosened steel bolt can be recognized by extracting the differential features provoked by bolt head rotation [22]. Researchers [23] have also applied spatial and morphological filters to extract depth-related deterioration features for a historic building in Italy. In a different study performed by Sangirardi *et al.* [24], a novel experimental methodology was employed by integrating motion minification and principal component analysis such that the crack pattern of a historic masonry wall can be identified in a laboratory configuration.

Despite the variety of computer vision algorithms discussed above, a commonality of these approaches is that vision-based algorithms are established, tested, and validated through digital images collected in the field. Due to the limitation of the camera's spatial resolution, the collected images usually cover limited regions of structures at a local scale (*e.g.*, a steel connection, a portion of a concrete floor, or a limited region of a building facade). Hence, these methods are ideal for identifying scattered damage spots in the historic structure. Transferring these

methods from the local scale to large-scale inspection (*e.g.*, full building façade, full bridge deck) could be challenging and is rarely attempted.

Furthermore, continuously monitoring the evolution of structural deterioration of historic structures over time is essential for owners and other stakeholders for their decision-making on repairs, retrofits, and rehabilitation. However, most of the existing vision-based SHM methods to date focus on damage detection based on the image data collected from a single field visit. Few studies in the literature attempt to align the image data from different field visits together and investigate how structural damage develops/evolves over time. This is probably due to the difficulties of aligning damage detection results of the same structural location against different inspections, as field images may be collected under different camera positions.

### 2.2. Photogrammetry-based SHM in cultural heritage

Photogrammetry is a technology for measuring information about a physical object and its surrounding environment by reconstructing a 3D model (*e.g.*, point cloud) from 2D digital images [25]. The concept of this technology has been first introduced by architect Albrecht Meydenbauer in 1867 for documenting a town church building [26] in Germany, and now has been widely applied in many engineering fields [27–30].

In terms of cultural heritage, photogrammetry is increasingly recognized as an effective engineering tool for reconstructing 3D models for documentation purposes. For example, Galantucci *et al.* [31,32] created a photogrammetry 3D model of a historic building in Italy and then created orthophotos of a building façade made of limestone blocks. As a result, the structural deterioration caused by cavities can be identified. Biscarini *et al.* [33] utilized UAV images of a historic masonry bridge to reconstruct the 3D model of the structure. The authors extracted orthophotos of the bridge deck and two bridge façades, based on which different bridge materials were further manually classified through human visual inspection. Forlin *et al.* [34] applied photogrammetry to extra orthophotos from the 3D models of a few archaeological sites in Cyprus and Spain, based on which earthquake-introduced crack patterns on the building's elevation walls can be identified.

Because photogrammetry-based 3D models contain enriched surface texture with high spatial resolution, these models show great promise to become ideal candidates for investigating the change/evolution of structural deterioration over time. By aligning two photogrammetry-based models into the same coordinate system, the differential features caused by structural deterioration can be uncovered. To this end, Ulvi [35] applied UAVs and photogrammetry to obtain 3D dense point clouds of an archaeological site in Turkey during four excavation phases, based on which elevation profiles of selected cut sections were extracted and compared. Galantucci *et al.* [36] proposed a health monitoring methodology to find material loss in a small area of a historic building façade. Nevertheless, these studies were mainly focused on investigating model changes in small-scale structural areas and/or geometric changes along 2D elevation profiles. Due to a lack of related data processing methodologies, large-scale and affordable monitoring approaches of historic structures over multiple inspection periods are rarely reported in the literature.

Recently, point cloud registration technologies have been applied to many engineering fields. Through the alignment of 3D dense point clouds under different inspection periods *via* computationally affordable algorithms, the differential features of the photogrammetry-based model (*i.e.*, point clouds) can be detected, localized, and quantified. For instance, Zhao *et al.* [37] leveraged UAVs and point cloud registration to monitor the damage evolution developed in reinforced concrete dams. The authors concluded that the proposed method is highly efficient and low-cost for the monitoring of the health conditions of dams. Jafari *et al.* [38] applied multi-view photogrammetry and point cloud registration in infrastructure health monitoring by detecting the deflection of a simply supported beam over time. With a detection accuracy of  $+/- 0.2$  mm, this method showed great potential for

geometric change detection in a variety of infrastructure inspection scenarios. Previously, the authors established a point cloud registration methodology for erosion monitoring of coastal cliffs [39]. The results of this study demonstrated the affordability and effectiveness of the proposed method for tackling large-scale complex engineering problems. Therefore, point cloud registration has shown great promise to be investigated in the field of health monitoring of historic structures.

### 2.3. Digital twin in cultural heritage

The concept of the digital twin is fast-evolving that has been applied to many engineering fields [40]. It is well agreed that the concept of the digital twin was presented by Grivevs in 2002 [41], and later Grivevs described the digital twin as a virtual representation of what has been produced [42]. In manufacturing engineering, Tao *et al.* [43,44] pointed out that a digital twin shall include five dimensions: physical part, virtual part, connection, data, and service. The physical and virtual parts represent the physical and virtual entities; the connection and data enable data transfer between physical and virtual entities; the digital twin must provide some services such as health monitoring and decision-making. Later on, Jiang *et al.* [45] adopted such a constituent of the digital twin when reviewing related studies in civil and infrastructure engineering. The authors further clarified that a digital twin connection only required data transfer from the physical entity to the virtual entity, while feedback in the reversed direction is not mandatory. In addition, the authors pointed out that the concept of the digital twin is different from the heritage building information model (HBIM) where an HBIM model does not require a physical entity or a connection between physical and virtual entities (although sometime an HBIM model may have these features).

In the field of cultural heritage, the digital twin has been adopted in different aspects. For example, Mohammadi *et al.* [46] built a digital twin of a steel truss bridge through two methods (photogrammetry and terrestrial laser scanning) and evaluated the accuracy of content creation of the digital twin. Marra *et al.* [47] created 3D virtual entities of two sculptures in the Archaeological Museum of the Ancient Capua in Italy. Finite element analyses were further carried out to calculate the vibration modes and stress distribution for preservation and maintenance purposes. Falcone *et al.* [48] investigated a digital twin of a historic building in Italy. The authors also discussed sensor data collection, processing for the virtual entity, and the framework for decision-making. In a similar study, a photogrammetry-based digital twin of a heritage monument was constructed by Themistocleous *et al.* [49].

However, the number of studies employing the concept of the digital twin in cultural heritage is limited and the full potential of the digital twin for generating new knowledge in cultural heritage still needs to be investigated. As reported by some related studies [45,50], the challenges of the adaptability of the digital twin in civil and infrastructure engineering lie in two aspects: 1) creating a high-fidelity virtual entity of the physical object; and 2) rapidly processing the collected data and performing diagnosis of the digital twin for decision-making. While some researchers in cultural heritage have addressed the first challenge by proposing photogrammetry-based reconstruction workflows to effectively build virtual models of historic structures, very few studies have attempted to leverage the digital twin as a framework for continuously monitoring time-varying structural deterioration.

### 3. Research gap

Based on the former realizations, there exists a clear research gap in the literature to develop a low-cost and effective methodology for the health monitoring of historic structures against time-varying deteriorations. As illustrated in Fig. 1a, while both computer vision-based and photogrammetry-based SHM methods have been well-studied in the literature for detecting damage in historic structures, the scopes of these methods are bound to detect structural health conditions at a given time.

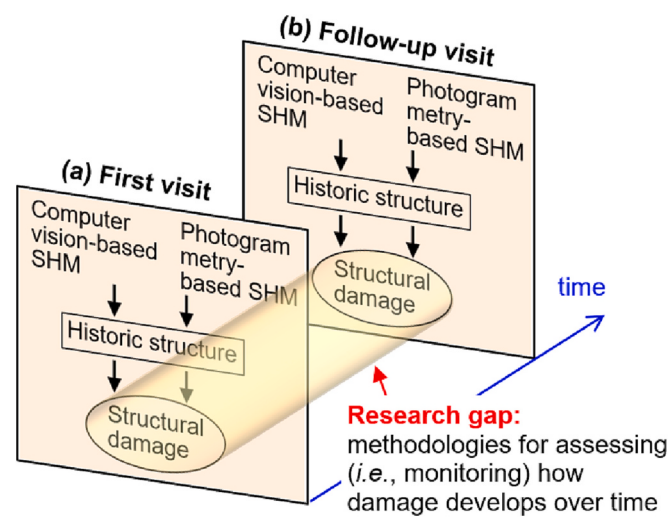


Fig. 1. A schematic to show the research gap.

Although an inspection team can repeat the same method for extracting damage to the historic structure after a time interval (e.g., the follow-up visit in Fig. 1b), the correlation of damage detected over different inspections has been rarely investigated. This study aims to fill this gap by investigating a novel methodology to document, examine, and monitor the development of structural deterioration over time.

The main technical contributions of this paper are three-fold:

First, different than most existing work in vision-based and photogrammetry-based SHM methods in cultural heritage, our method focuses on detecting deterioration developed over different inspections by aligning virtual models together to extract the differential features provoked by structural damage. Such time-varying information, once available, makes it possible to obtain the physical state of damage development/evolution in a historic structure. Therefore, the results produced by the proposed method are highly valuable to owners and other stakeholders in their decision-making on routine maintenance, repair, retrofit, or rehabilitation. The existing work in the literature has difficulties addressing this challenge.

Second, most existing methods in both vision-based and photogrammetry-based SHM can only identify damage that occurs at scattered spots on historic structures at a local scale due to the limited camera's spatial resolution and/or image processing software capacities. These methods are insufficient for scanning/mapping structural health conditions at a large scale. In contrast, the method we propose in this study shows the viability of health monitoring at different scales. The sensing capability for a much larger structural area than existing methods makes the proposed method become an effective engineering tool for the health monitoring of historic structures.

Third, we adapt a digital twin framework for the structural deterioration diagnosis of historic structures. The virtual models established in our study contain both enriched geometric and RGB textured information of the physical entity under different time states. Therefore, the virtual models themselves can be treated as the dataset for monitoring the health conditions of historic structures. Although some existing studies leverage frameworks of the digital twin for SHM in civil infrastructure, few investigations focus on the geometric aspect of the digital twin to directly extract geometric differentiated features provoked by time-varying damage. Our investigation extends the knowledge of the digital twin from this perspective, particularly in the context of cultural heritage preservation.

## 4. Methodology

### 4.1. Overview of the proposed digital twin framework

**Fig. 2** illustrates the proposed digital twin framework for bridge health monitoring. Here we follow the definition of digital twin proposed by Jiang *et al.* [45] and establish a five-dimension digital twin framework including the physical part, virtual part, service, dataset, and connections. The physical part (**Fig. 2a**) is a historic structure that is prone to structural deterioration with multiple time-varying physical states (*i.e.*, deterioration develops over time). Accordingly, the virtual part (**Fig. 2a**) contains the corresponding virtual models reconstructed for each physical state of the structure using the dataset (UAV images) in **Fig. 2d**. The service in this study represents the structural damage detection and monitoring for stakeholders and owners of their decision-making (**Fig. 2c**). Finally, connections (**Fig. 2e**) are enabled throughout the proposed framework for allowing data to be transferred between each digital twin dimension.

The proposed framework starts with the initial visit to the historic structure to collect UAV images of the structure. This can be achieved by a portable digital camera with a tripod or an onboard UAV camera through a preprogrammed flight. Protocols for UAV operation and image collection can be found in **Section 4.2**. Next, photogrammetry-based structure-from-motion with multi-view stereo (SfM-MVS) algorithms are adopted to create the initial virtual model of the historic structure (see **Section 4.3**). Due to the complex geometry layout of the physical entity, a dedicated 3D reconstruction procedure is established via Agisoft Metashape [51] that includes 1) filtering out low-fidelity point clouds using a pre-defined cutoff threshold; and 2) constructing point clouds of different bridge segments and then register/merge them into one virtual model. Once the virtual model of the bridge is established, it contains both geometric and RGB textured representations of the physical entity.

To extract the time-varying structural deterioration, a follow-up visit is carried out at a later time (**Fig. 2a**) and UAV images of the historic structure are collected accordingly (**Fig. 2d**). An updated virtual model

(**Fig. 2b**) reflecting the new structural conditions is then reconstructed via the same SfM-MVS protocols (see **Section 4.3**). Next, both initial and updated virtual models are transferred to the service domain (**Fig. 2c**) for detecting and monitoring structural deterioration. To this end, a Region of Interest (ROI) is first selected from both virtual models. Then the initial and updated virtual models are truncated to fit the ROI's size. Thereafter, a novel health monitoring methodology is established (**Fig. 2c**) to align/register the truncated virtual models (initial and updated) together with a two-stage alignment procedure in Cloud-Compare [65]. Once aligned, point cloud processing algorithms are proposed to identify the geometric changes occurring during different inspections. A detailed discussion of the above tasks can be found in **Section 4.4**. Based on the damage detection results, the owners and stakeholders can deliberate the decisions on possible actions in maintenance, retrofit, or rehabilitation.

Notice that the physical part is subjected to time-varying physical states (*i.e.*, development of structural deterioration). To extract the differential features provoked by the structural damage, at least two virtual models representing two physical states are required. This allows the proposed health monitoring methodology (**Fig. 2c**) to examine the differential geometric features extracted from the two virtual models. Although this paper only shows the results based on two field visits, the digital twin framework itself is an iterative procedure and can be easily extended to monitor the health status of the historic structure over the long term. This can be achieved by running the loop of the digital twin framework (*i.e.*, performing additional field visits; building corresponding virtual models; transferring the data among different digital twin dimensions for bridge health monitoring and decision-making). Lastly, this study focuses on data collection of the physical entity, building high-fidelity virtual models, and developing the bridge health monitoring method for detecting time-varying structural damage; while investigation of decision-making for site owners and other stakeholders is out of the scope of this paper.

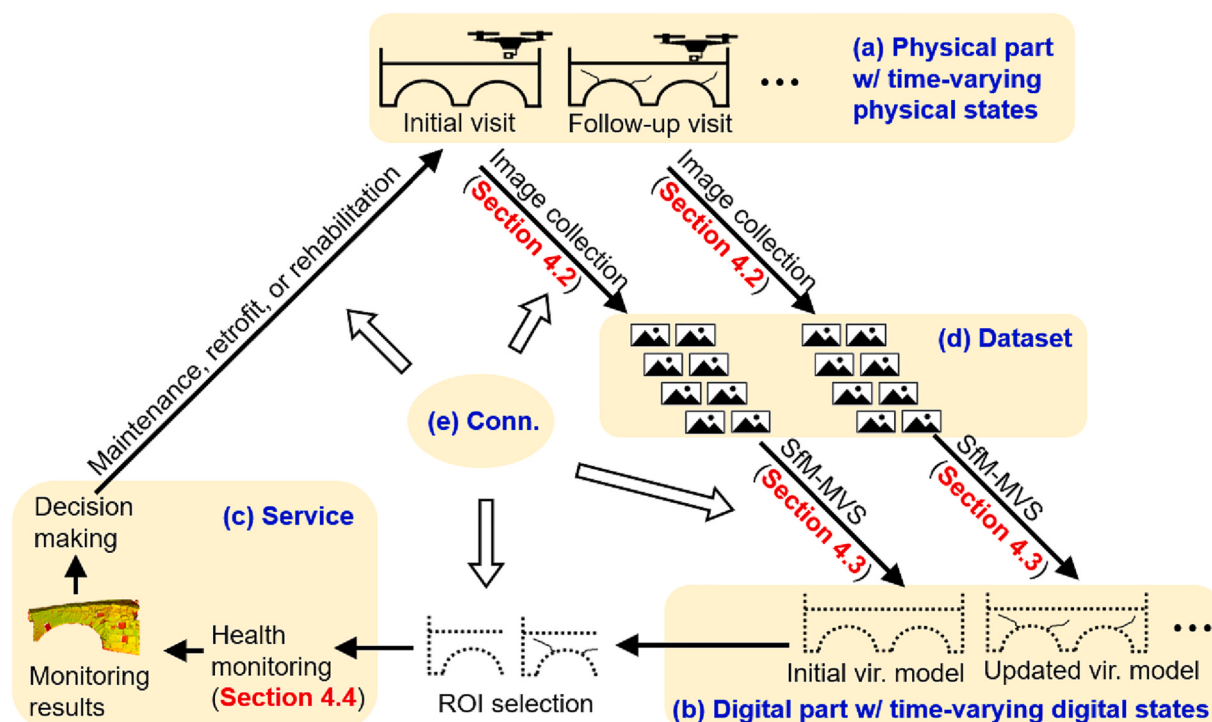


**Fig. 2.** The proposed digital twin framework for bridge health monitoring: (a) physical part; (b) digital part; (c) service; (d) dataset; and (e) connections.

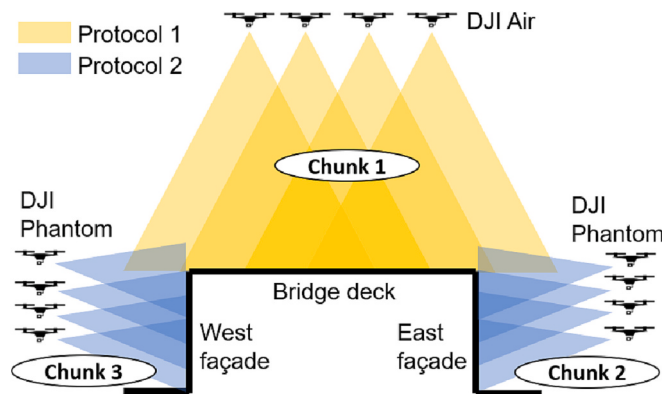


**Fig. 3.** Two protocols for UAV operation and image collection.

#### 4.2. UAV operation and image collection

**Fig. 3** shows the strategies of UAV operation and image collection in the field. The strategies overall are to ensure the collected UAV images can cover all external surfaces of the bridge under different camera positions with sufficient image overlapping. To make it viable, two protocols are established during both field visits (initial and follow-up) which govern the UAV operations and image collections. The protocols are further explained as follows:

- The first protocol (*i.e.*, the yellow pattern in **Fig. 3**) is to take a series of aerial images to scan the bridge deck from the top of the bridge. This is realized by manually operating the DJI Air to automatically take images with an interval of 2 s. The flying speed of the DJI Air is intentionally limited to ensure adjacent images collected can share enough overlapping areas (about 80% overlapping). The altitude of the flight is limited between 5 and 10 m above the elevation of the bridge deck.
- The second protocol (*i.e.*, the blue patterns in **Fig. 3**) is to operate the DJI Phantom 4 Pro+ V2.0 (DJI Phantom hereafter) and collect images on the bridge's façades separately. Like the previous protocol, the UAV images also are taken using 2 s intervals. The flight altitude and the camera shooting distance vary depending on the need. For example, some UAV images capture large portions of the bridge façade under longer shooting distances and higher altitudes; other UAV images may capture detailed structural conditions of stones under shorter shooting distances and lower altitudes.

#### 4.3. Virtual model reconstruction via SfM-MVS

A photogrammetry workflow is proposed in this study to create the virtual models of the bridge. Here we use a sample sculpture (see **Fig. 4**) to briefly illustrate this procedure. To start, a large volume of digital images of the sculpture are collected by cameras under different camera positions with extensive image overlapping. Next, collected images are processed by a workflow with SfM-MVS algorithms [52,53]. Such a

workflow begins with detecting feature points across all field images. Feature points (see **Fig. 4a**) are small image patches that contain unique intensity distributions which are invariant against image rotation, translation, and scaling. Feature points that consistently appear through multiple images are detected, aligned, and paired. The 3D coordinates of paired feature points along with their camera parameters can be also established during this stage, based on which a sparse point cloud can be created as shown in **Fig. 4b**. Sparse point cloud reconstruction requires less computational cost but can still offer a reliable initial alignment of field images. In this regard, users can easily evaluate the quality of image alignment, identify potential outliers (*i.e.*, incorrect alignments), and examine the distribution of feature points. Thereafter, image pixels are back-projected to all images to reconstruct an RGB-colored dense point cloud, as shown in **Fig. 4c**. The dense point cloud serves as the virtual model of the sculpture. For a comprehensive review of SfM-MVS and 3D reconstruction, the reader is referred to [54,55] regarding the recent advances of these technologies for cultural heritage.

Because the historic Bridge in this study has a complex geometric layout, directly reconstructing the bridge from all UAV images collected from the field visit could be challenging and prone to alignment errors. Here we propose a new approach to guide the image reconstruction (**Fig. 5**). Briefly, the UAV images of the bridge are first grouped into three chunks based on the inspection areas. As illustrated in **Fig. 3**, Chunk 1 contains images taken by DJI Air to cover the bridge deck area; while Chunks 2 and 3 refer to images taken by DJI Phantom to cover the east and west façades of the bridge, respectively. Thereafter, a sparse point cloud and a dense point cloud are established at each chunk as shown in **Fig. 5a** and b. Because noise contents are inevitably induced in this procedure, dense points with fewer reconstruction confidences shall be removed. Here we adopt a built-in filter in Agisoft Metashape [51] with a predefined threshold to automatically eliminate noisy feature points (**Fig. 5c**). Lastly, the filtered dense point clouds at each chunk are aligned together to form the final dense point cloud (*i.e.*, the virtual model) of the bridge (**Fig. 5d**), serving as the virtual model in the proposed digital twin framework.

#### 4.4. Bridge health monitoring

**Fig. 6** illustrates the methodology of bridge health monitoring which includes ROI segmentation, rough point cloud alignment, fine point cloud alignment, and damage detection. The methodology starts with ROI segmentation by truncating both the initial and updated virtual models (*i.e.*, point clouds) into the size defined by ROI. Sizing virtual models to fit ROI allows for reducing computational efforts while only focusing on specified areas of interest. In this study, an ROI is defined as an area from the historic structure where the owners and stakeholders are interested in learning its health condition for purposes of maintenance, retrofit, or rehabilitation. With variable dimensions, ROIs could be a bridge deck/façade at a large scale; a portion of the bridge that is prone to damage at a small scale (*e.g.*, a specified area in the bridge deck with a high risk of cracking; or a connection in bridge pier that is prone to damage); or a mesoscale with area's dimensions in between. For illustration purposes, ROI is selected as one of the bridge façades in the

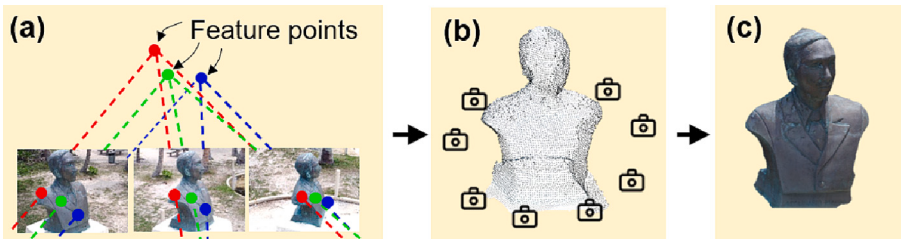


**Fig. 4.** A physical entity can be reconstructed as a virtual entity *via* a photogrammetry-based SfM-MVS workflow. (a) Feature points that consistently appear in images shot under different camera positions; (b) reconstructed sparse point cloud; and (c) reconstructed dense point cloud.

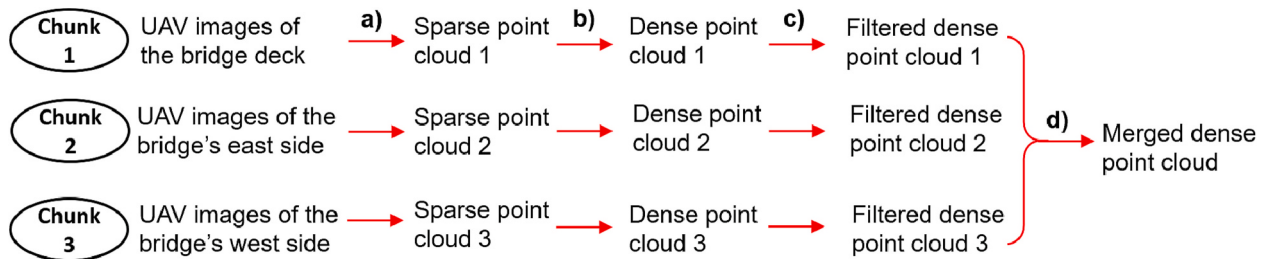


**Fig. 5.** Overview of the procedure for virtual model reconstruction: a) sparse point cloud reconstruction; b) dense point cloud reconstruction; c) point cloud filtering; and d) merge of individual dense point clouds.

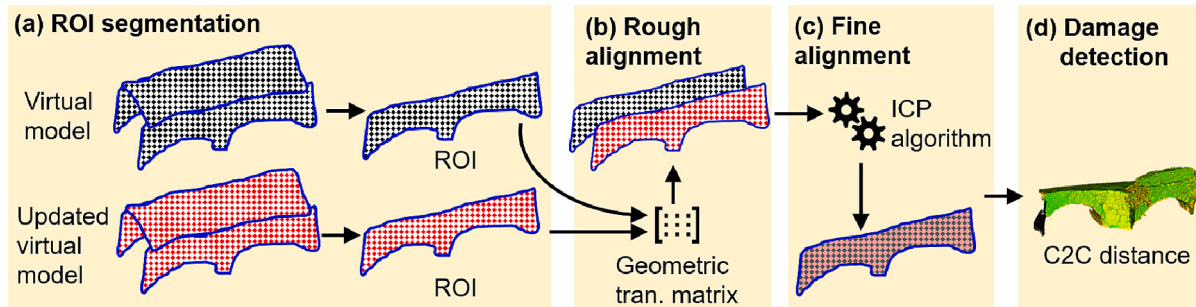


**Fig. 6.** Methodology of bridge health monitoring: (a) ROI segmentation; (b) rough point cloud alignment; (c) fine point cloud alignment; and (d) damage detection.

context of this discussion as shown in Fig. 6a.

Next, we apply a two-stage point cloud registration protocol to find the geometric similarities between the initial and updated virtual models under ROI. To start, we first perform a rough point cloud alignment (see Fig. 6b) by manually selecting a minimum of three correspondences from both virtual models. Correspondences are 3D points that are visually distinguishable by human eyes and are located at similar locations in both models. For example, a 3D point with a unique color intensity pattern that consistently appears in both models can be the candidate for correspondence selection (*e.g.*, corners of the stones, intersections of the stone's bed joints, stain marks). The 3D coordinates of selected correspondences do not need to be accurate at this stage. Based on correspondences, a geometric transformation matrix is established which contains a translation and rotation (three degrees of freedom of translation; three degrees of freedom of rotation) to align one virtual model to another.

Due to position errors in manually selecting correspondences, improvement is needed for the accurate alignment of the virtual models (*i.e.*, point clouds). Here we adopt the iterative closest point (ICP) algorithm [56,57] to further optimize the geometric transformation matrix (see Fig. 6c). To explain, we consider the segmented point cloud under ROI from the initial virtual model as the reference cloud (see black

color bridge façade in Fig. 6b); the segmented point cloud from the updated virtual model as the floating cloud (see red color bridge façade in Fig. 6b). For each point in the floating point cloud, the closest point in the reference point cloud is identified by finding the minimum point-to-point distances. Once all points from the float point cloud are evaluated, a geometric transformation matrix is estimated using a root mean square point-to-point distance metric minimization technique, which can be expressed as the equation below [38]:

$$E(R, t) = \min_{R, t} \sum_i \|p_i - (Rq_i + t)\|^2 \quad (1)$$

where  $R$  and  $t$  are the rotation and translation from the geometric transformation matrix to be applied to the float point cloud;  $E(R, t)$  is the error function;  $p_i$  is a point from the reference point cloud; and  $q_i$  is a point from the floating point cloud. Then, the established geometric transformation matrix is applied to the floating point cloud to align it with the reference point cloud. Once the floating point cloud is aligned to a new position, the above procedure is repeated by finding the new optimized geometric transformation matrix for the next round of alignment until the iteration converges.

Lastly, we differentiate the model geometric change by calculating the cloud-to-cloud (C2C) distance (Fig. 6d). To this end, we denote two

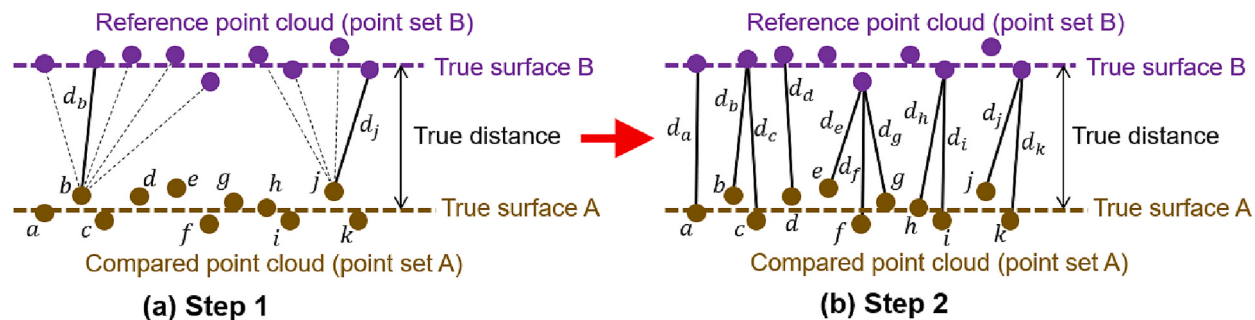


**Fig. 7.** The schematic of the C2C distance calculation. (a) For each point in the compared point cloud, the nearest point in the reference point cloud is searched and its minimum distance is calculated (*i.e.*,  $d_b$  and  $d_j$ ). (b) Once all points in the compared point cloud have been evaluated for their minimum distances, the C2C distance is the maximum distance from  $d_a$  to  $d_k$ . The figures are modified from [59] and [60].

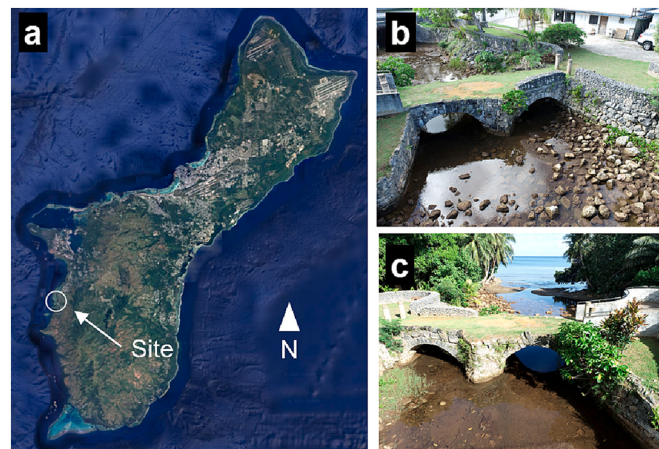


**Fig. 8.** Overview of the Taleyfac Spanish Bridge: a) location of the bridge on the island of Guam from Google Maps; b) the west side of the bridge, and c) the east side of the bridge.

point sets:  $A = \{a_1, \dots, a_p\}$  for the reference point cloud and  $B = \{a_1, \dots, a_q\}$  for the floating point cloud. The Hausdorff distance of two point sets is defined as [58]:

$$H(A, B) = \max(h(A, B), h(B, A)) \quad (2)$$

where  $h(A, B) = \max_{a \in A} \min_{b \in B} \|a - b\|$ . The function  $h(A, B)$  ranks each point of point set  $A$  based on its distance to the nearest point of point set  $B$ , and then applies the largest ranked point as the final distance. If structural deterioration causes any changes in the geometric shapes in the physical entity of the bridge, it would be documented in the updated virtual model and further provoke an abrupt C2C distance. Therefore, structural deterioration developed during the inspection period can be identified by the proposed bridge health monitoring methodology.

Fig. 7 illustrates the schematic of the C2C distance calculation where point set  $A$  is the compared point cloud and point set  $B$  is the reference point cloud. For each point in the compared point cloud, the nearest point in the reference point cloud is searched and the corresponding minimum distance is identified. Here we select Points  $b$  and  $j$  in Fig. 7a, among all possible point-to-point distances,  $d_b$  and  $d_j$  are the minimum distances for these two points. The same evaluation procedure is applied for every other point in the compared point cloud. As a result, the minimum distances for all points in the compared point cloud have been

solved as illustrated in Fig. 7b. Finally, the C2C distance is defined as the maximum distance from  $d_a$  to  $d_k$  in Fig. 7b. Notice that C2C distance calculation is insensitive to cloud density. The Hausdorff distance can be obtained regardless of cloud density distributions.

## 5. Validation

### 5.1. Study site

To verify the proposed method, we selected the Taleyfac Spanish Bridge (Tollai Taleyfak in Chamorro) in the United States Territory of Guam. Being the largest island from the Marianas Chain located in the Western Pacific, Guam has an ancient history with a rich cultural heritage. To date, there are 132 National Register of Historic Places in Guam spread across 17 of 19 villages of the island, as recognized by the United States federal government [61]. Despite the support from the federal and local governments, challenges still exist in the preservation of historic structures in Guam using traditional structural inspection practices. This is mainly due to the difficulty in hiring trained technicians (e.g., licensed engineers) for performing routine inspections, as well as the limited resources to secure advanced sensing platforms and learn sensing technologies (e.g., vibration sensors, load pressure cells, and environmental sensors). As discussed in this paper, the proposed digital

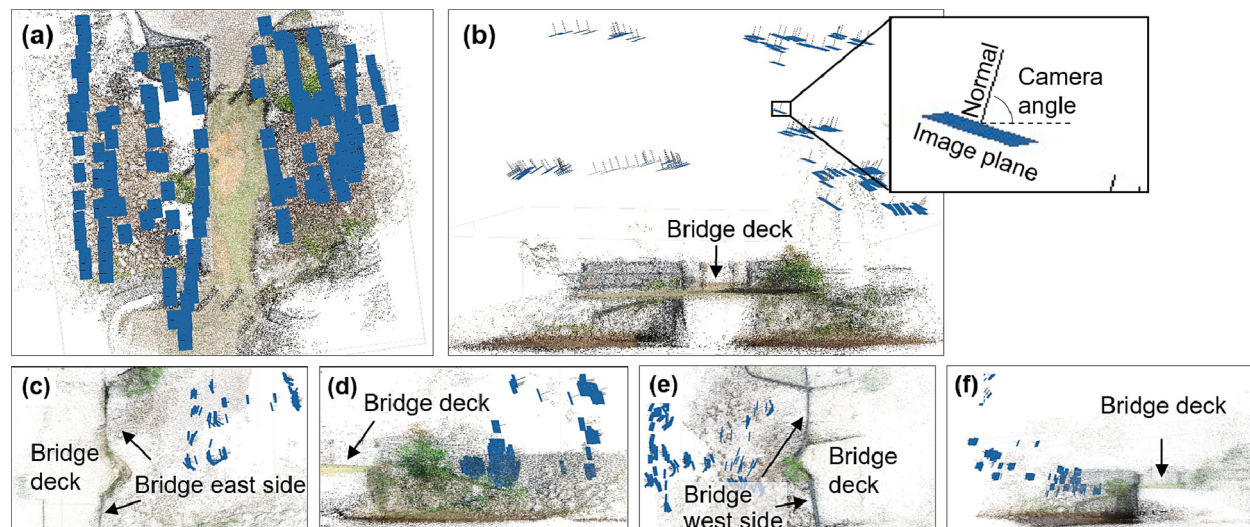


**Fig. 9.** The camera positions under Protocols 1 and 2 during the initial visit. (a) and (b) are plan and elevation views for images of the bridge deck; (c) and (d) are plan and elevation views for images of the bridge east façade; and (e) and (f) are plan and elevation views from images of the west façade.

twinning approach only relies on off-the-shelf UAVs and affordable and/or open-source software, significantly reducing the implementation cost. Therefore, underrepresented cultural heritage communities with limited resources like Guam would benefit from the proposed method.

The Taleylac Spanish Bridge is located in the Village of Agat in Guam and is on the west side of the island (Fig. 8a). The bridge orients in the north-south direction and can be accessed from both ends through two walk-in platforms (Fig. 8b and c). The bridge is one of the most photographed and visited historic sites on the island of Guam and is one of two double-arched stone bridges in the Mariana Islands [62]. This bridge was originally constructed of wood in 1785 for the river crossing of the road that linked the village of Agana and the southern region of the island (*i.e.*, Apra Harbor and the village of Umatac). In 1866, the original bridge was demolished due to severe deterioration and replaced by a stone arch bridge. Because the replacement occurred during Spanish rule, the best architecture at this time was meant to show power and authority [63]. Therefore, the bridge was rebuilt using large rectangular precise hard-cut stones without any layers of plaster, leaving a greater sense of structural integrity.

After the Spanish-American War in 1898, the bridge was governed by the United States Navy for transportation (*e.g.*, motor vehicles, pack animals, wagons, and troops) until 1917 [62]. After the war, the bridge traffic became obsolete and the bridge was no longer used for its original purpose. In the nomination form submitted to the United States National Register of Historic Places in 1974 [64], the bridge was described as in a deteriorating condition with a portion of the south arch missing. In the next few decades, the bridge was subjected to other assaults caused by floods, storms, and earthquakes. In 2013, the bridge was restored with the support of the Gaum Preservation Trust.

The bridge has both significant technical and historical values [62]. First, stone arch bridges like the Taleylac Bridge built without present-day structural engineering technologies (*i.e.*, steel, reinforced concrete) are a legacy of the past and thus the historical engineering information provided by the bridge is valuable. Second, the bridge's historical value relates to the heritage of the people of Guam and the Spanish infrastructural legacy of road systems connecting their towns and villages.

## 5.2. UAV operation and image collection

An initial field visit was carried out on the Taleylac Bridge on June 28th in 2020. The UAV deployment work was performed at the north

platform of the bridge (see the platform on the right side of the bridge in Fig. 8c), close to the parking spots near Guam Highway 2. Fig. 9 shows camera positions (blue patches) from UAV images. To better illustrate the location of cameras, sparse point clouds of the bridge are also shown in the figure. These UAV images are collected under the two protocols defined in Fig. 3 where Protocol 1 collects images of the bridge deck (see Fig. 9a and b) and Protocol 2 collects the images of both bridge façades (see Fig. 9 c to f).

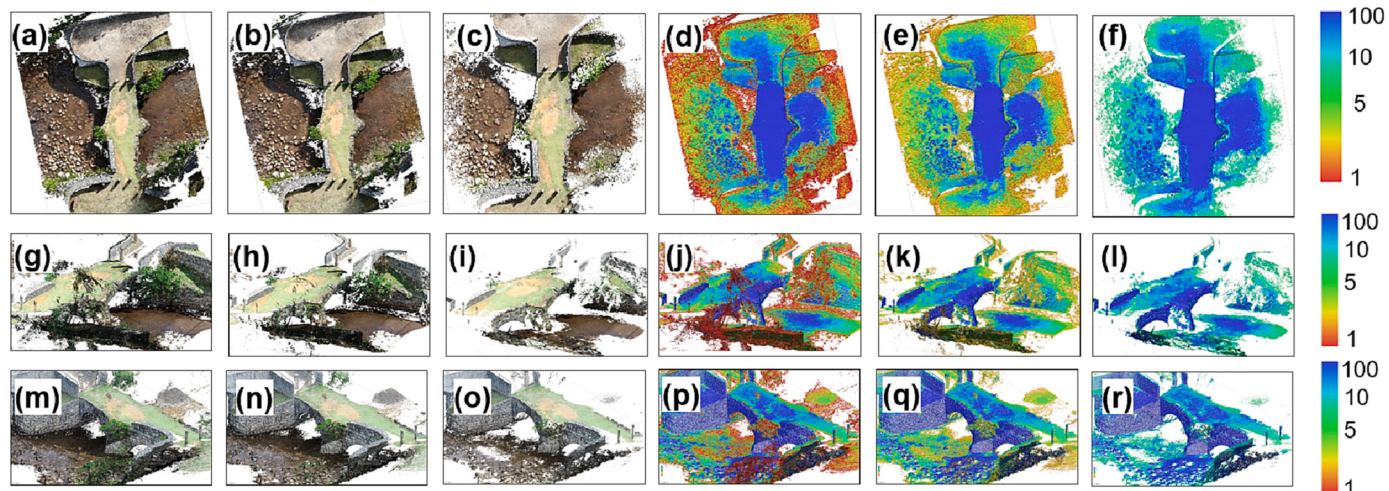
As shown in Fig. 9a, multiple short flights are carried out along the longitudinal direction of the bridge. While some flights are directly over the top of the bridge deck; other flights are shifted laterally on both east and west sides of the bridge. This allows the UAV camera to capture a portion of both the bridge façades. In addition, instead of using a straight-down camera view (*i.e.*, 90 degrees camera angle), the onboard UAV camera was tilted up slightly with a camera angle between 45 and 70 degrees (the camera angle is defined in Fig. 9b). This ensures suitable views to film the details of both bridge façades. Fig. 9c to f show the camera positions from UAV images capturing both bridge façades. 156, 141, and 193 UAV images are collected from the bridge deck (Fig. 9a), east façade (Fig. 9c), and west façade (Fig. 10e).

A follow-up visit to the bridge was carried out on July 18th, 2020. The strategies for UAV operation and image collection are the same as the initial visit. Due to the limited space, the camera positions from the follow-up visit are reported in Appendix A.

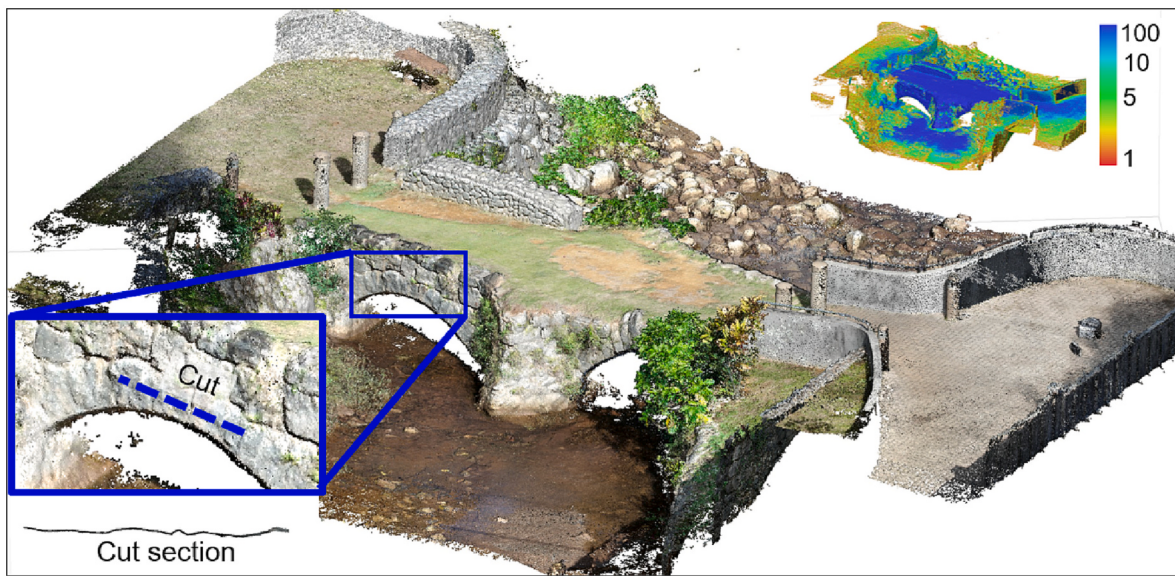
## 5.3. Virtual model reconstruction via SfM-MVS

Fig. 10 shows the interim reconstruction results for each image chunk for the initial visit. Each row of Fig. 10 refers to results generated by the UAV images from a specified chunk. The first column in Fig. 10 represents the unfiltered RGB textured point clouds; the second column represents filtered RGB textured point clouds after filtering out points with point confidence of less than 1; the third column represents filtered RGB textured point clouds after filtering out points with point confidence of less than 5. The last three columns in Fig. 10 are the same results as the first three columns but are under contour plots to show the point confidence distributions. Point confidence is a unitless parameter in Agisoft Metashape that presents the reconstruction error with a range from 0 to 100.

As can be seen from Fig. 10, the points with high confidence (blue zone) are located around the bridge deck in Chunk 1; the east façade in Chunk 2; and the west façade in Chunk 3. This is because such high-



**Fig. 10.** Summary of image reconstruction where the 1st, 2nd, and 3rd rows are the reconstruction results based on images from Chunks 1, 2, and 3, respectively. The 1st and 4th columns are point clouds without filtering; the 2nd and 5th columns are point clouds after filtering out points with confidences less than 1; the 3rd and 6th columns are point clouds after filtering out points with confidences less than 5. Colors in a), b), and c) are real RGB colors extracted from field images; d), e), and f) are contour plots against point confidence.



**Fig. 11.** The final RGB textured dense point cloud serves as the virtual model from the initial visit. The contour plot of confidence for the same point cloud is shown in the top right corner. A magnified view of the bridge's arch and its profile along the cut section are shown in the bottom left corner.

confidence areas have been repetitively captured by the field UAV images with extensive image overlapping during the field visit. In addition, with a higher threshold of the point confidence filter, more 3D points can be filtered out. This has been verified from data from Chunk 1 (Fig. 10e and f), as well as the data from Chunks 2 and 3 (Fig. 10k and l; Fig. 10q and r).

Once the dense point cloud of the individual chunk has been established, a predefined cutoff threshold (point confidence = 1) is applied to each point cloud to filter out the low-confidence points. Thereafter, the filtered dense point clouds are aligned together in Agisoft Metashape to produce the final dense point cloud of the bridge. Fig. 11 shows the final dense point cloud that serves as the initial virtual model in the proposed digital twin framework. Notice that both bridge façades and the deck are reconstructed with high fidelity (see blue zones in the contour plot in the top right corner of Fig. 11). The bottom left corner of the figure also shows the magnified view of one arch on the east façade where a cut section is applied to the stones. The point cloud profile of the cut section has been shown in the figure.

The updated virtual model from the follow-up visit is reconstructed *via* a similar procedure. Due to the limited space, the final reconstruction result is reported in Appendix B.

#### 5.4. Bridge health monitoring

To monitor the health condition of the bridge, we select the ROI as the entire bridge's west façade. Then, both virtual and updated virtual models (*i.e.*, point clouds) are truncated to fit the area of the selected ROI. Fig. 12 shows the truncated point clouds from both initial and updated virtual models under the ROI. Thereafter, a total of four correspondences are manually selected from both models in CloudCompare [65]. R0 to A3 (Fig. 12a) are correspondences on the point cloud from

the initial visit; A0 to A3 (Fig. 12b) in the same correspondences on the point cloud from the follow-up visit. These correspondences allow a geometric transformation matrix to be estimated, based on which the two point clouds can be roughly aligned together. Thereafter, the fine alignment is performed using the ICP algorithm. Finally, aligned point clouds are scaled into the correct real-world unit using ground truth measurements of the bridge dimensions taken from the engineering drawings of the latest bridge's retrofit in 2013.

The C2C distances of the two point clouds under ROI are calculated as shown in Fig. 13a. As can be seen from the figure, the C2C distances are generally small between the two point clouds. To further evaluate C2C distances of localized areas, we select four locations and further magnify their views in Fig. 13b to e. These locations are three stone surfaces at the bridge's façade denoted as Locations A, B, and C (see Fig. 13a); and an area of the plant on the edge of the bridge deck at mid-span denoted as Location D.

The histograms of the C2C distances of the bridge façade of these four locations are further illustrated in Fig. 14. Because the follow-up field visit was shortly after the initial visit, little or no structural deterioration can be expected during such a short period. This can be confirmed by observing the histograms of the C2C distance of the entire façade (Fig. 14a), where most C2C distances of the façade are concentrated around 0.01 m (Fig. 14b). Considering that the bridge has an entire length of 10.7 m, such an error is about  $0.01 \text{ m} / 10.7 \text{ m} = 0.09\%$  of the bridge's overall dimension. In terms of three locations taken from the stone surface (Fig. 14c to e), their histograms have shown a similar trend with most of the C2C distances being around 0.01 m. The last location around the plant (*i.e.*, Location D), however, produces much higher C2C distances (Fig. 14f), indicating large reconstruction errors. This is caused by the difficulty of SfM-MVS algorithms in reconstructing thin-type objects [66].

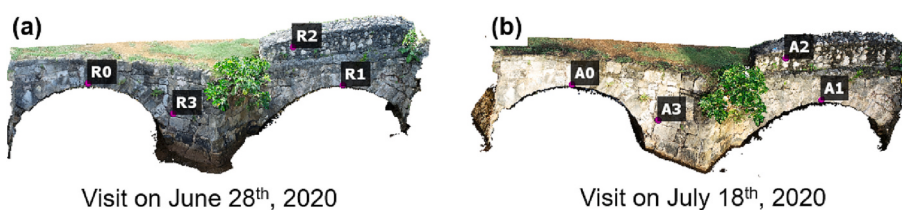


**Fig. 12.** (a) and (b) are truncated point clouds under the selected ROI for both initial and follow-up visits.

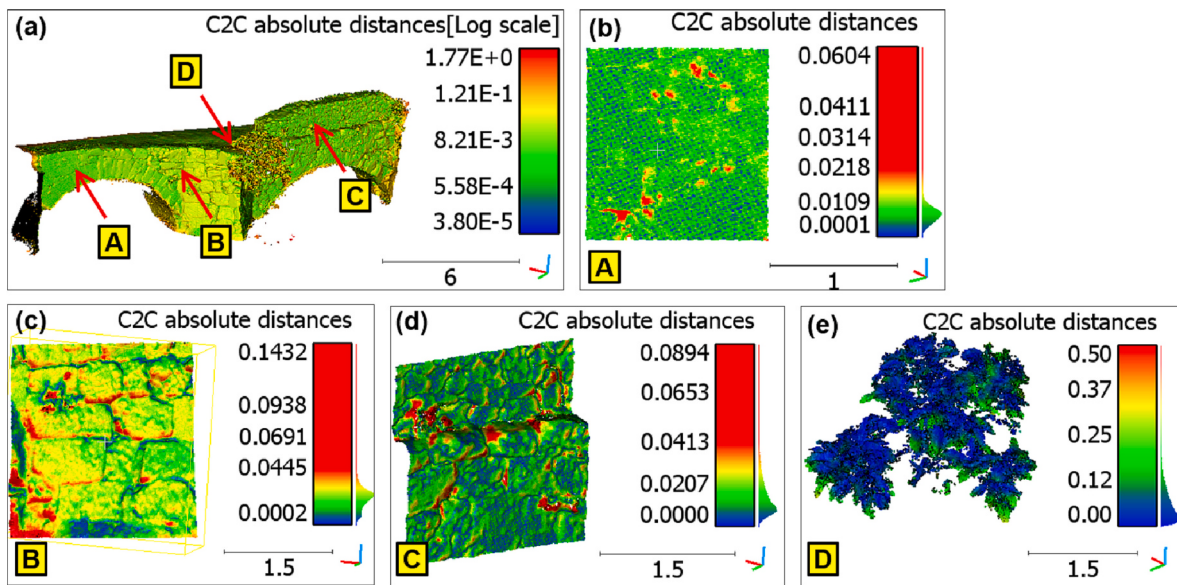


**Fig. 13.** (a) C2C distances between point clouds from the initial and follow-up; (b) to (e) are magnified views of C2C distances for four locations denoted in (a). The unit of all figures is  $m$ .

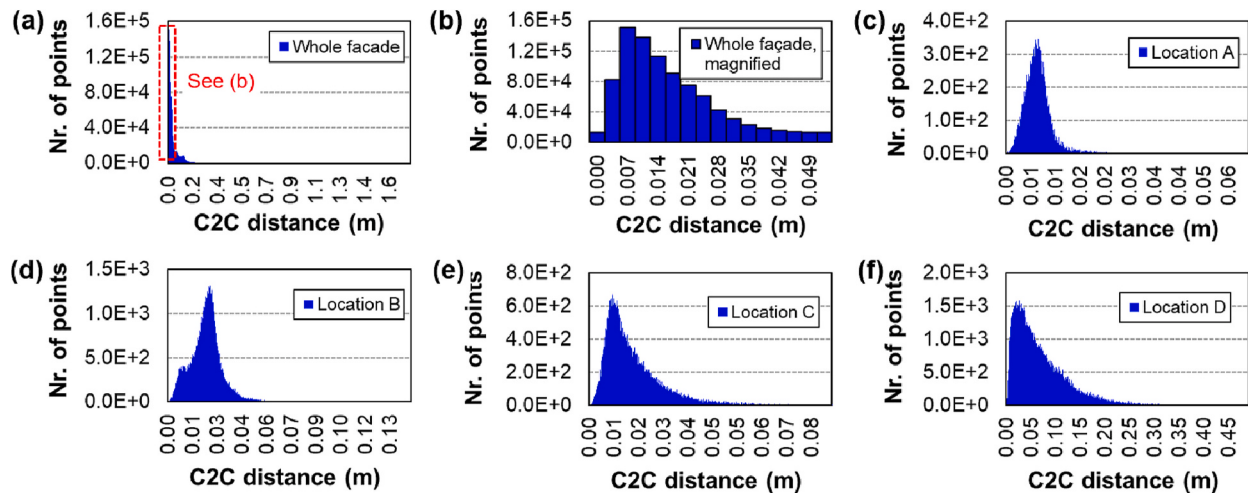


**Fig. 14.** Histograms of the C2C distances from: (a) the whole façade; (b) a magnified view of (a); (c) Location A; (d) Location B; (e) Location C; and (f) Location D.

## 6. Health monitoring on simulated structural deterioration

Because the duration between the initial and follow-up field visits was relatively short, no structural deterioration was detected in Section 5. Therefore, we further explore the viability of the proposed method for detecting simulated structural deteriorations. To accommodate this, a revised bridge health monitoring methodology will be first explained in this section. Thereafter, the validations of the proposed method in detecting three simulated structural deteriorations (*i.e.*, loosened stones, a surface crack, and an uneven settlement) will be discussed in the rest of Section 6.

Fig. 15 illustrates the revised bridge health monitoring methodology modified from Fig. 6. To explain, let us assume the initial and updated virtual models have been reconstructed via SfM-MVS (Fig. 15a and c). Next, an ROI is defined and both point clouds from the initial and updated virtual models have been truncated to fit the size of the ROI (Fig. 15b and d). To mimic the structural deterioration that one would see in reality, we quantify one or multiple regions in the point cloud of ROI from the updated virtual model (Fig. 15d) to be considered structural damage. This could, for example, be loosened stones on the bridge

façade, cracking patterns on the bridge surface, or uneven settlements on the bridge deck. Thereafter, the point cloud (Fig. 15d) is segmented into two parts: the point cloud contains all damage features (Fig. 15e), and the point cloud of the remainder structure (Fig. 15f). Because the location of structural damage is known *a priori*, the ground truth of damage can be directly obtained from the procedure of point cloud segmentation in this step (Fig. 15i). Then, we merge point clouds of damage features (Fig. 15e) and the remainder of the structure (Fig. 15f) to form the updated point cloud (Fig. 15g). This new point cloud (Fig. 15g) contains simulated structural deterioration and is further compared with the point cloud of the same ROI generated from the initial virtual model (Fig. 15b). Through the algorithms explained in Section 4.4, the structural deterioration can be detected and monitored as shown in Fig. 15h. The results of the blocks highlighted in orange (*i.e.*, Fig. 15 g, h, and i) will be illustrated later in this section.

Three types of structural deterioration are simulated including loosened stones, a surface crack, and an uneven settlement at the bridge deck. Fig. 16 illustrates the selections of ROIs for each type of structural damage. Blue ROI A is selected as a portion of the bridge's west façade where four stones are loosened; Red ROI B is selected as the bottom area

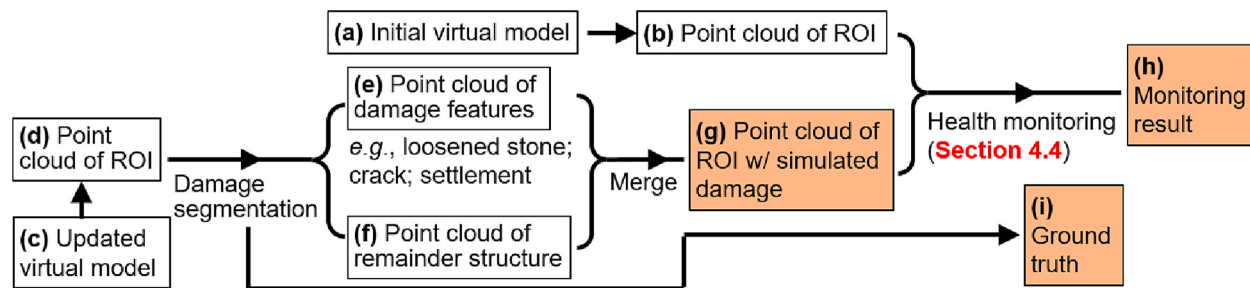


**Fig. 15.** Revised methodology for bridge health monitoring. The results of the blocks highlighted in orange for each type of structural deterioration will be illustrated later in this section. (For interpretation of the references to color in this figure legend, the reader is referred to the web version of this article.)

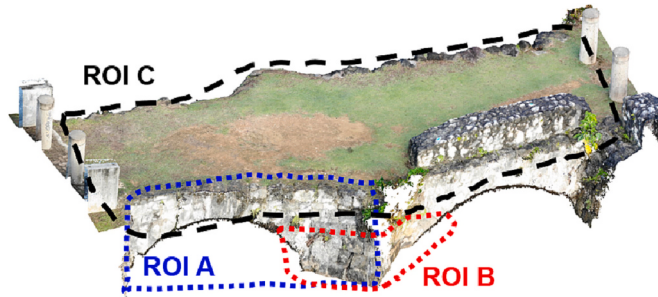


**Fig. 16.** ROI selections for loosened stones (blue dashed lines); a surface crack (red dashed lines); and an uneven settlement (black dashed lines). (For interpretation of the references to color in this figure legend, the reader is referred to the web version of this article.)

of the bridge's middle pier where a surface diagonal crack is simulated; Black ROI C is selected as the bridge deck which contains a simulated uneven settlement.

#### 6.1. Stone loosening detection

Loosening stones and falling stone blocks are the most common structural deterioration occurring in stone or masonry structures [67]. Detecting loosened stones at an early stage, therefore, becomes critical to evaluate the health condition of the bridge such that retrofit can be performed on time. Here we select one arch from the west façade as the ROI (see Fig. 17a). Inside this ROI, we further quantify four stones in the bridge façade that are loosened during the inspection period. Next, the surfaces of these four stones are segmented from the remainder of the wall and moved along the positive normal direction (i.e., the direction

that is perpendicular to the wall) as denoted in magnified Patch A (Fig. 17b). This simulates the loosening behavior of the stones between the initial and follow-up visits.

The proposed method successfully identifies the correct loosened stones at multiple locations over the bridge façade wall through the revised health monitoring approach (Fig. 17f) and agrees well with the ground truth measurements (Fig. 17g). Notice that the detection result is based on the differentiated geometry information generated from datasets of two field visits (the bridge's digital twin created from the initial visit vs. the point cloud with simulated damage obtained from the follow-up visit). Due to the lack of reference information, the loosened stones would not be detected from the follow-up visit alone. In this regard, existing vision-based and/or photogrammetry-based SHM methods would likely fail in detecting the loosened stones compared with our proposed method, as most of them only utilize a single dataset.

Fig. 18 shows the histogram of the C2C distance from the ROI (i.e., bridge surface in Fig. 17a). Most C2C distances are concentrated around 0.01 m which is consistent with the observation in Section 5. However, different than the distribution in Fig. 14a and b, extra plateaus appear at a higher C2C distance (see the magnified view from the figure). This is provoked by the discrepancies between the bridge's digital twin created from the initial visit and the simulated point cloud with loosened stones in the follow-up visit. The four loosened stones between two inspections induce geometric discrepancies and this has been successfully identified by the histogram.

#### 6.2. Crack detection

Surface cracks on stone or masonry walls are a major threat to structural integrity [68,69]. To mimic a cracking pattern on the bridge's stone wall, we select a portion of the bridge façade as ROI (shown in Fig. 19a). Within the ROI, we induce a surface crack at the bottom of the

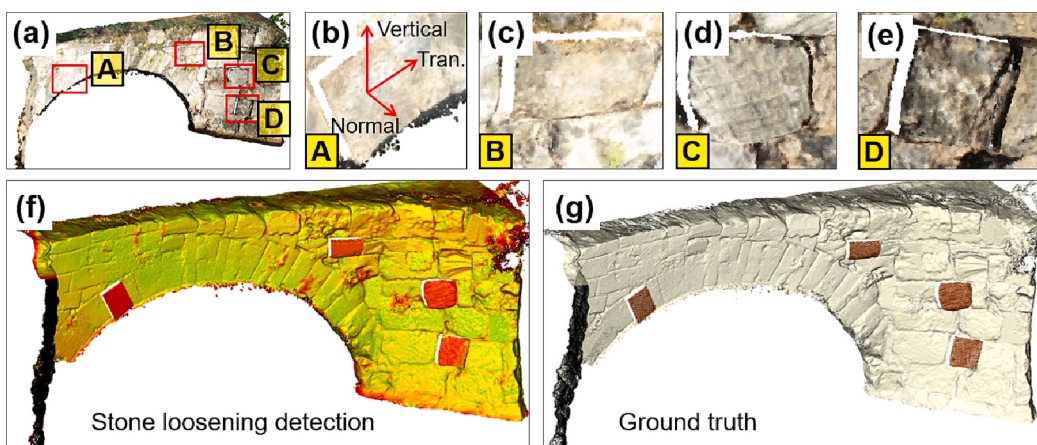


**Fig. 17.** (a) The point cloud of the ROI that includes loosened stones; (b) to (e) magnified views of the loosened stones; (f) detection result of loosened stones; and (g) ground truth measurements.

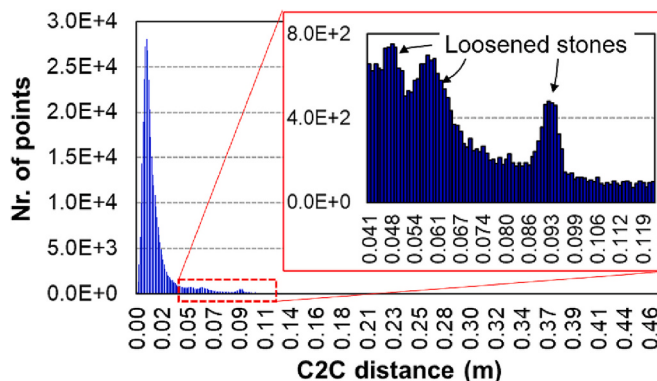


Fig. 18. Histogram of the C2C distances of the ROI.

bridge pier. This diagonal crack across three levels of stone layers is created by segmenting the point cloud of ROI into a crack-like thin surface area and the remainder of the structure. Next, this segmented thin surface area is slightly moved along the negative normal direction (see Fig. 19c) to simulate the depth area provoked by cracking that one would see in reality.

Since the procedure of crack segmentation is known as *a priori*, the ground truth measurement of the crack can be directly established during this procedure and is further shown in Fig. 19f and g. Through the

revised bridge monitoring method (Fig. 15), the crack detection result is illustrated in Fig. 19d and e. A good agreement can be identified between the detection result and the ground truth measurement. Notice that the crack is solely simulated based on a geometric change of the stone surface while the RGB color information is not altered.

Two histograms for the C2C distances are shown in Fig. 20. Fig. 20a is the histogram of the C2C distances under the ROI (i.e., the bridge surface in Fig. 19a); Fig. 20b is the histogram of the C2C distances under the image patch defined in Fig. 19b. As the crack is a localized damage that only propagates along the surface of a few stones, the special pattern provoked by the crack can not be seen in the histogram of the ROI (Fig. 20a). A different phenomenon, however, can be observed from the histogram of a small image patch under cracking (see Fig. 20b). Some of the C2C distances in this image patch are around 0.054 m caused by cracking.

### 6.3. Uneven settlement

An ROI of the bridge deck is selected for simulating the uneven settlement as shown in Fig. 21a. The black dashed line in Fig. 21a refers to the settlement area. Inside this ellipse area, the point cloud is further segmented into four ring-shaped point clouds (see rings a to d denoted in Fig. 21c) along with the remainder of the structure. Next, these segmented ring-shaped point clouds are slightly moved downward. To mimic the uneven settlement, the middle of the settlement area contains the largest downward movement compared with the area far away from

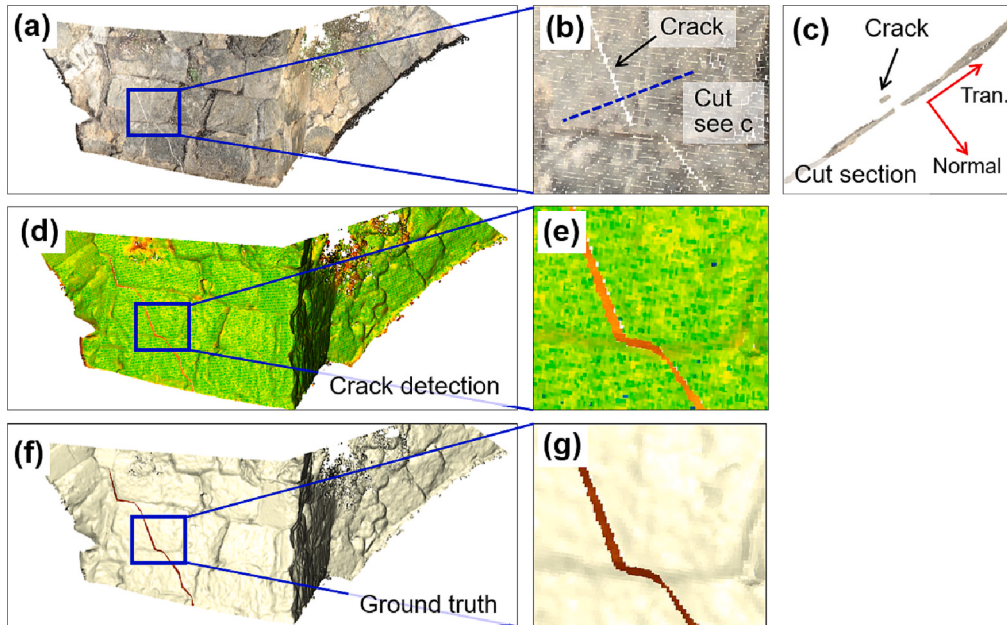


Fig. 19. (a) The point cloud of the ROI that includes a surface crack; (d) detection result of the crack; (f) ground truth measurement; (b), (e), (g) magnified views; (c) profile along the cut defined in (b).

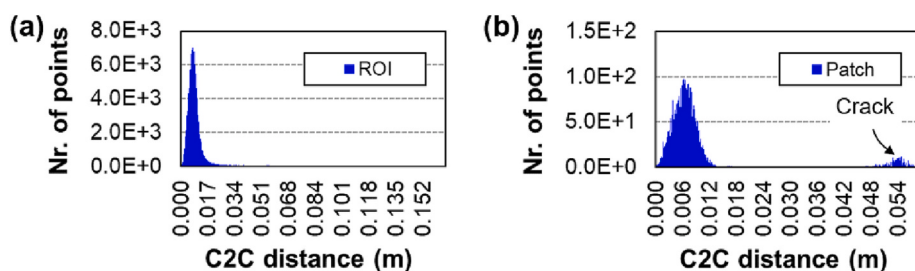
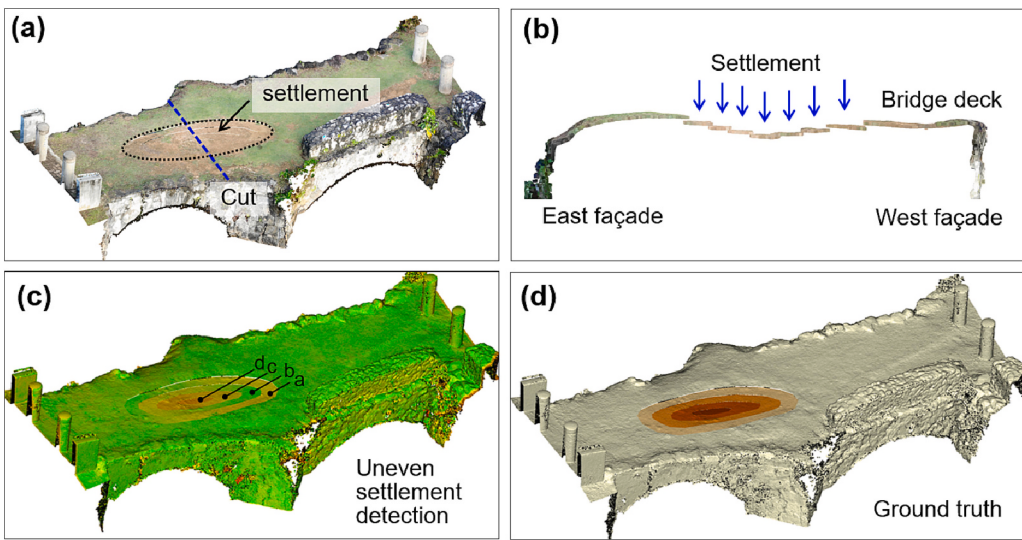


Fig. 20. (a) Histogram of the C2C distances of the ROI; (b) histogram of the C2C distances of the image patch as identified in Fig. 19b.



**Fig. 21.** (a) The point cloud of the ROI that includes an uneven settlement on the bridge deck; (b) elevation profile along the cut (*i.e.*, blue dashed line) defined in (a); (c) detection result of the uneven settlement; and (d) ground truth measurement. (For interpretation of the references to color in this figure legend, the reader is referred to the web version of this article.)

the center (see the blue arrows in Fig. 21b). Thereafter, the updated point cloud is merged and compared with the bridge's digital twin established from the initial field visit.

Fig. 21c illustrates the settlement detection result, from which a deformed area can be identified with different color patterns to indicate the amount of settlement. This result is further compared against the ground truth measurement directly created from the point cloud segmentation (Fig. 21d). Both results are generally agreed with each other. Notice that five colors can be found from the ground truth measurement including gray from the remainder of the structure; and yellow, orange, red, and dark red from four ring-shaped areas with different amounts of settlement. These different colors do not quantify the magnitude of the settlement. Instead, they solely represent the ground truth boundaries of segmented point clouds before.

Two histograms of the C2C distances are shown in Fig. 22. Fig. 22a is the histogram of the C2C distances under the ROI (*i.e.*, the bridge surface in Fig. 21a); Fig. 22b is the histogram of the C2C distances under the ellipse area defined by the black dashed line in Fig. 21a. As the uneven settlement occurs in a localized area in the bridge deck, it does not provoke any significant pattern in the histogram of the whole ROI (see Fig. 22a). However, if the evaluation area is reduced to the ellipse area, a few plateaus can be observed across the horizontal axis (see Fig. 22b). These are caused by the settlements of different ring-shaped point clouds.

## 7. Discussions

### 7.1. Viability

Results in Sections 5 and 6 verified the viability of the proposed method in detecting structural deterioration at multiple scales. These range from local scale (crack detection in Section 6.2), mesoscale (loosened stones detection in Section 6.1), and large scale (uneven settlement detection in Section 6.3 and results in Section 5). The successes of these investigations validate the viability of the proposed approach to health monitoring of the historic structure. Existing vision-based SHM methods, on the other hand, strongly relies on the special resolution of input images hence would be difficult to uncover structural damage over a mesoscale and/or large scale. Although high-resolution cameras or image stitching techniques may be adopted to overcome this issue, the project implementation and computational costs would be increased accordingly. Also, the proposed digital twin framework in this study would work for point cloud data obtained by other means such as LiDAR and/or laser scanners. Many LiDAR/laser scanning instruments equipped with digital cameras which can automatically register RGB information to the point clouds. The obtained point clouds, in this regard, are similar to the point clouds generated via SfM-MVS shown in this study. Therefore, these point clouds would be suitable for being processed by the proposed bridge health monitoring method and the digital twin framework.

### 7.2. Adaptability

The proposed approach in this study can be easily adopted/adapted

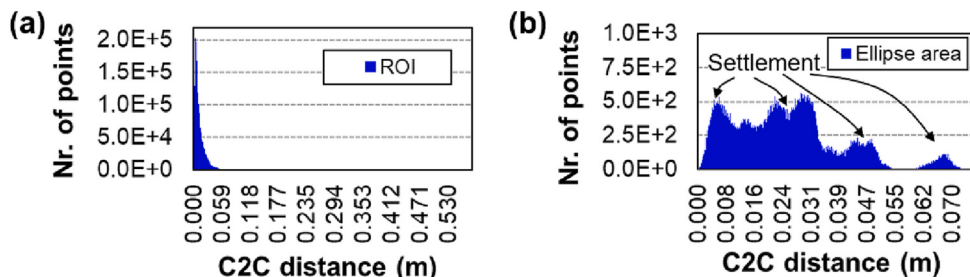


**Fig. 22.** (a) C2C distances of the ROI; and (b) C2C distances of the ellipse area as identified by the black dashed line in Fig. 21a.

by owners and stakeholders of historic structures, particularly ones from underrepresented communities with cultural preservation needs. Quite often, these underrepresented communities struggle with limited resources (e.g., difficulties in hiring qualified inspection personnel; insufficient budgets in obtaining engineering tools for inspection). The market prices of DJI Air and DJI Phantom 4 used in this study were about \$500 and \$2400, respectively. Considering these UAVs can be reused for different projects, obtaining these UAVs is relatively affordable. The hardware in this study for building the bridge's virtual models and processing the point clouds is a workstation (4.8GHz CPU; 32GB RAM). The software adopted in this study is either off-the-shelf (*i.e.*, Agisoft Metashape) or open-source at no cost (*i.e.*, CloudCompare). Compared to traditional physical sensor-based methods that require labor-intensive work in field deployment or computer vision-based SHM methods based on training machine learning algorithms, the proposed method would substantially reduce the implementation cost when being adopted/adapted by underrepresented communities to a different cultural heritage preservation project. Lastly, in terms of the computational cost, the processing time in Agisoft Metashape for generating the dense point cloud for one image chunk ranges from one to two hours using the aforementioned workstation, depending on the number of UAV images and other software setting configurations. The implementation of the bridge health monitoring method in CloudCompare does not require any significant waiting time.

### 7.3. Limitations

A limitation of the proposed method lies in the robustness of building the point cloud against the structural surface covered by plants. Stone surfaces covered with green plants are prone to reconstruction error (see the plant at the bridge's midspan in Fig. 10p). Accordingly, the accuracy of C2C distance around this area is negatively affected with an average C2C distance error of 0.05 m (see Fig. 13f). This is due to the limitation of photogrammetry-based SfM-MVS algorithms in reconstructing thin-type objects [66]. Therefore, the proposed method may not work well for assessing a historic structure that has been heavily covered by plants. Also, the GPS signals beneath the bridge arches may be weak and the lighting conditions in these areas are dark. For these reasons, operating UAVs beneath the bridge arches have not been attempted in the field visits. Lastly, the average C2C distance error of the bridge in this study is found to be 0.01 to 0.02 m (see Fig. 13b to e) for structure surfaces without plant coverage. In this regard, the proposed method may not distinguish any subtle changes that are provoked by C2C distances of less than 0.02 m. Using a laser scanning technique [70] could help to improve registration accuracy. Similar point cloud registration errors also exist in other investigations [37,46,71].

## 8. Conclusions

This paper presents a new research methodology for health monitoring of historic structures through photogrammetry technologies and digital twinning. The state-of-the-art of computer vision-based and photogrammetry-based SHM methods, the recent trend of digital twin applications in cultural heritage, and the research gap have been discussed. Thereafter, the methodological framework of the proposed approach has been introduced and then validated through the Taleyfac Spanish Bridge on the United States Territory of Guam. Results show the successes of building high-fidelity virtual models of the bridge *via* SfM-MVS, as well as the feasibility of bridge health monitoring. To further extend the potential of this proposed framework, a revised bridge health monitoring methodology is established to detect simulated structural damage including loosened stones on the bridge's façade, a surface

crack, and an uneven settlement on the bridge deck. Results verify the viability of the proposed method in identifying different types of structural deteriorations. Finally, the flexibility of the proposed approach in detecting damage at different scales, the adaptability of the proposed method for different cultural heritage projects, and the limitations of the proposed method are summarized.

Overall, the investigation results of this study have shown great promise to document/detect structural damage; and monitor the development of damage over time. Such time-varying information, as enabled by the proposed digital twin framework, may not be available from many existing computer vision-based and photogrammetry-based SHM methods. The findings of this study also illustrate a new insight into leveraging the digital twin in health monitoring of historic structures in the cultural heritage community. Once virtual models of the historic structure are established using the image data from a longer period, they can be used for damage diagnosis purposes over the long term. In addition, although the scope of this study is in the domain of historic structures, the proposed methodology could be extended for SHM of other types of structures (e.g., infrastructure, buildings, and highway bridges). Lastly, this study investigates the digital twin framework in terms of data collection of the physical entity, building high-fidelity virtual models, and developing the bridge health monitoring method for detecting time-varying structural damage; while the study of decision-making based on monitoring results is out of the scope of this paper.

## Funding

This study is based on work supported by the NASA Guam EPSCoR under award No. 80NSSC19M0044 issued through the NASA EPSCoR Program in the United States. The first author is also partially supported by the new faculty research start-up fund from the Gupta College of Science at Coastal Carolina University. However, any opinions, findings, conclusions, or recommendations expressed in this study are those of the authors and do not necessarily reflect the views of the funders.

## Declaration of Competing Interest

The authors declare that they have no known competing financial interests or personal relationships that could have appeared to influence the work reported in this paper.

## Data availability

Data will be made available on request.

## Acknowledgement

We thank undergraduate student assistant Angela Maglaque at the University of Guam for assisting in field visits; engineering students James Rhodes, Eric Cantley, Nathan Dempski, and Jermaine Gadsden at Coastal Carolina University for performing the investigation of this project through their capstone project *via* ENGR 499 Senior Design; the Guam NASA EPSCoR program and the Research Corporation of the University of Guam (RCUOG) for managing the fund; the Office of Research and Sponsored Programs (ORSP) at the University of Guam for supporting a portion of the equipment used in this study. We appreciate the constructive comments from Dr. William Ambrose at Coastal Carolina University and anonymous reviewers, which improve the quality of this manuscript. Finally, we thank Lea Quinitio, John Borja, Dr. Leslie Aquino, Dr. Romina King at the University of Guam, and Joe Quinata from the Guam Preservation Trust.

## Appendix A

**Fig. 23** shows the camera positions of the follow-up visit under Protocols 1 and 2. 202, 78, and 50 UAV images are collected from the bridge deck (**Fig. 23a**), east façade (**Fig. 23c**), and west façade (**Fig. 23e**), respectively

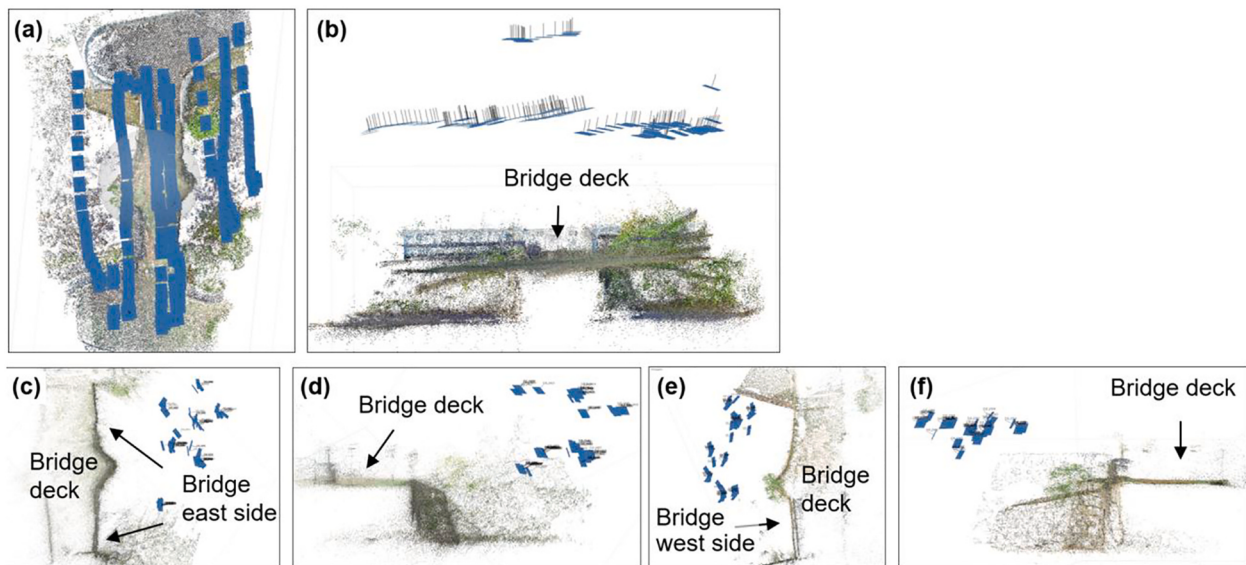


**Fig. 23.** The camera positions under Protocols 1 and 2 during the follow-up visit. (a) and (b) are plan and elevation views for images of the bridge deck; (c) and (d) are plan and elevation views for images of the bridge east façade; and (e) and (f) are plan and elevation views from images of the west façade.

## Appendix B

**Fig. 24** shows the final reconstructed dense point cloud from the follow-up visit, serving as the updated virtual model in the proposed digital twin framework. Because UAVs are operated around sunset without ideal lighting conditions, the UAV images contain a higher noise floor than the ones taken from the initial field visit. To compensate for this, a higher cutoff threshold (point confidence = 5) is adopted in Agisoft Metashape to remove the points with low point confidence. The result in the figure is the point cloud after applying this filter

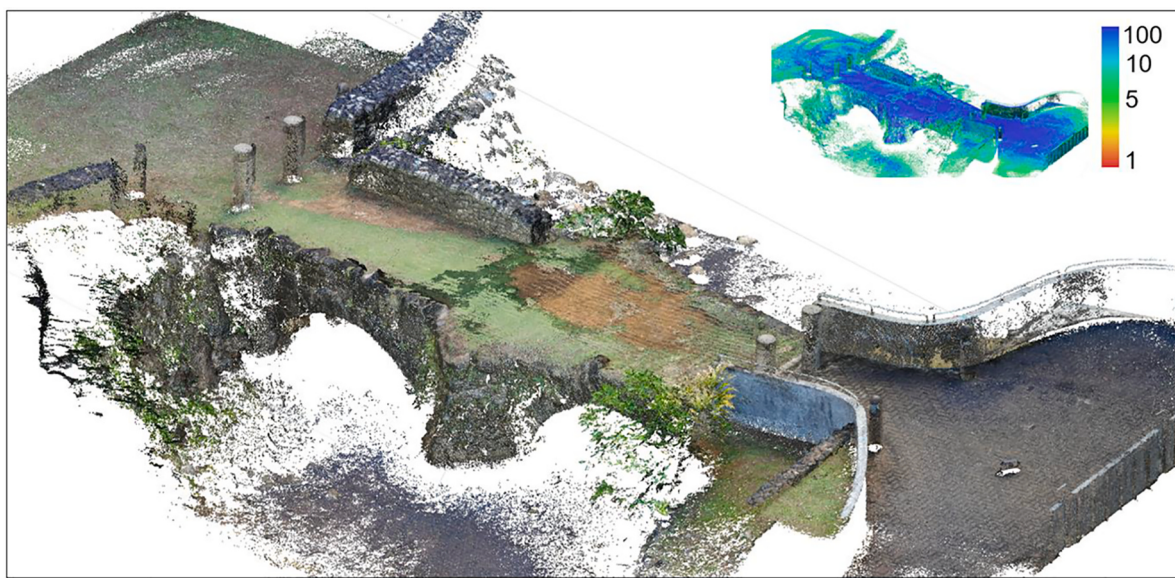


**Fig. 24.** The final RGB textured dense point cloud serves as the updated virtual model from the follow-up visit. The contour plot of confidence for the same point cloud is shown in the top right corner.

## References

- [1] A. Belal, E. Shcherbina, Heritage in post-war period challenges and solutions, IFAC-PapersOnLine 52 (25) (2019) 252–257, <https://doi.org/10.1016/j.ifacol.2019.12.491>.
- [2] S.L. Farhan, V.S. Akef, Z. Nasar, Revitalizing the historical center of Al-Najaf city in Iraq: learning from the British conservation experiences, J. Cult. Heritage Manag.
- Sustain. Develop. 12 (4) (2022) 513–532, <https://doi.org/10.1108/JCHMSD-01-2020-0002>.
- [3] E. Hammer, R. Seifried, K. Franklin, A. Lauricella, Remote assessments of the archaeological heritage situation in Afghanistan, J. Cult. Herit. 33 (2018) 125–144, <https://doi.org/10.1016/j.culher.2017.12.008>.
- [4] L.E.S. Coleman, Official response to the Russian war crimes in Ukraine, Curator: The Museum J. 65 (2022) 15–16, <https://doi.org/10.1111/cura.12483>.

- [5] M. Vatan, Condition survey of historic buildings by visual inspection-case study: Murat pasha mosque, *Int. J. Electron. Mech. Mechatron. Eng.* 2 (1) (2012) 147–156. [https://ijemme.aydin.edu.tr/wp-content/uploads/2020/04/ijemme\\_v2\\_i1008.pdf](https://ijemme.aydin.edu.tr/wp-content/uploads/2020/04/ijemme_v2_i1008.pdf) (date of last access: 02/18/2023).
- [6] A. De Stefano, E. Matta, P. Clemente, Structural health monitoring of historical heritage in Italy: some relevant experiences, *J. Civ. Struct. Heal. Monit.* 6 (1) (2016) 83–106, <https://doi.org/10.1007/s13349-016-0154-y>.
- [7] M. O’Shea, J. Murphy, Design of a BIM integrated structural health monitoring system for a historic offshore lighthouse, *Buildings* 10 (7) (2020) 131, <https://doi.org/10.3390/buildings10070131>.
- [8] V. Gattulli, M. Lepidi, F. Potenza, Dynamic testing and health monitoring of historic and modern civil structures in Italy, *Struct. Monit. Mainten.* 3 (1) (2016) 71, <https://doi.org/10.12989/smm.2016.3.1.071>.
- [9] F. Ubertini, G. Comanducci, N. Cavalagli, Vibration-based structural health monitoring of a historic bell-tower using output-only measurements and multivariate statistical analysis, *Struct. Health Monit.* 15 (4) (2016) 438–457, <https://doi.org/10.1177/1475921716643948>.
- [10] M.G. Masciotta, L.F. Ramos, P.B. Lourenço, The importance of structural monitoring as a diagnosis and control tool in the restoration process of heritage structures: a case study in Portugal, *J. Cult. Herit.* 27 (2017) 36–47, <https://doi.org/10.1016/j.culher.2017.04.003>.
- [11] H. Blanco, Y. Boffill, I. Lombillo, L. Villegas, An integrated structural health monitoring system for determining local/global responses of historic masonry buildings, *Struct. Control. Health Monit.* 25 (8) (2018), e2196, <https://doi.org/10.1002/stc.2196>.
- [12] Z. Zou, X. Zhao, P. Zhao, F. Qi, N. Wang, CNN-based statistics and location estimation of missing components in routine inspection of historic buildings, *J. Cult. Herit.* 38 (2019) 221–230, <https://doi.org/10.1016/j.culher.2019.02.002>.
- [13] N. Wang, X. Zhao, Z. Zou, P. Zhao, F. Qi, Autonomous damage segmentation and measurement of glazed tiles in historic buildings via deep learning, *Comput.-Aided Civil and Infrastruct. Eng.* 35 (3) (2020) 277–291, <https://doi.org/10.1111/mice.12488>.
- [14] L.E. Mansuri, D.A. Patel, Artificial intelligence-based automatic visual inspection system for built heritage, *Smart Sustain. Built Environ.* 11 (3) (2022) 622–646, <https://doi.org/10.1108/SASBE-09-2020-0139>.
- [15] R. Pathak, A. Saini, A. Wadhwa, H. Sharma, D. Sangwan, An object detection approach for detecting damages in heritage sites using 3-D point clouds and 2-D visual data, *J. Cult. Herit.* 48 (2021) 74–82, <https://doi.org/10.1016/j.culher.2021.01.002>.
- [16] E. Hatır, M. Korkanç, A. Schachner, İ. İnce, The deep learning method applied to the detection and mapping of stone deterioration in open-air sanctuaries of the Hittite period in Anatolia, *J. Cult. Herit.* 51 (2021) 37–49, <https://doi.org/10.1016/j.culher.2021.07.004>.
- [17] M. Mishra, Machine learning techniques for structural health monitoring of heritage buildings: a state-of-the-art review and case studies, *J. Cult. Herit.* 47 (2021) 227–245, <https://doi.org/10.1016/j.culher.2020.09.005>.
- [18] G. Wang, W.T. Peter, M. Yuan, Automatic internal crack detection from a sequence of infrared images with a triple-threshold canny edge detector, *Meas. Sci. Technol.* 29 (2) (2018), 025403, <https://doi.org/10.1088/1361-6501/aa9857>.
- [19] D. Reagan, A. Sabato, C. Niziozrecki, Feasibility of using digital image correlation for unmanned aerial vehicle structural health monitoring of bridges, *Struct. Health Monit.* 17 (5) (2018) 1056–1072, <https://doi.org/10.1177/1475921717735326>.
- [20] A. Akagic, E. Buza, S. Omanovic, A. Karabegovic, Pavement crack detection using Otsu thresholding for image segmentation, in: 2018 41st International Convention on Information and Communication Technology, Electronics and Microelectronics (MIPRO), IEEE, 2018, May, pp. 1092–1097, <https://doi.org/10.23919/MIPRO.2018.8400199>.
- [21] X. Kong, J. Li, Non-contact fatigue crack detection in civil infrastructure through image overlapping and crack breathing sensing, *Autom. Constr.* 99 (2019) 125–139, <https://doi.org/10.1016/j.autcon.2018.12.011>.
- [22] X. Kong, J. Li, Image registration-based bolt loosening detection of steel joints, *Sensors* 18 (4) (2018) 1000, <https://doi.org/10.3390/s18041000>.
- [23] R.A. Galantucci, F. Fatiguso, Advanced damage detection techniques in historical buildings using digital photogrammetry and 3D surface analysis, *J. Cult. Herit.* 36 (2019) 51–62, <https://doi.org/10.1016/j.culher.2018.09.014>.
- [24] M. Sangirardi, V. Altomare, S. De Santis, G. de Felice, Detecting damage evolution of masonry structures through computer-vision-based monitoring methods, *Buildings* 12 (6) (2022) 831, <https://doi.org/10.3390/buildings12060831>.
- [25] B.A. DeWitt, P.R. Wolf, *Elements of Photogrammetry (With Applications in GIS)*, 2000. ISBN: 9780071761123.
- [26] J. Albertz, Albrecht Meydenbauer-Pioneer of photogrammetric documentation of the cultural heritage, *Int. Arch. Photogramm. Remote. Sens. Spat. Inf. Sci.* 34 (5/C7) (2002) 19–25. [http://www.theulegium.de/fileadmin/user\\_upload/Texte/Meydenb.pdf](http://www.theulegium.de/fileadmin/user_upload/Texte/Meydenb.pdf) (date of last access: 02/18/2023).
- [27] I. Colomina, P. Molina, Unmanned aerial systems for photogrammetry and remote sensing: a review, *ISPRS J. Photogramm. Remote Sens.* 92 (2014) 79–97, <https://doi.org/10.1016/j.isprsjprs.2014.02.013>.
- [28] M. Pepe, L. Fregonese, M. Sciaioni, Planning airborne photogrammetry and remote-sensing missions with modern platforms and sensors, *Eur. J. Remote Sens.* 51 (1) (2018) 412–436, <https://doi.org/10.1080/22797254.2018.1444945>.
- [29] H. Omar, L. Mahdjoubi, G. Kheder, Towards an automated photogrammetry-based approach for monitoring and controlling construction site activities, *Comput. Ind.* 98 (2018) 172–182, <https://doi.org/10.1016/j.compind.2018.03.012>.
- [30] A. Braun, A. Borrmann, Combining inverse photogrammetry and BIM for automated labeling of construction site images for machine learning, *Autom. Constr.* 106 (2019), 102879, <https://doi.org/10.1016/j.autcon.2019.102879>.
- [31] R.A. Galantucci, F. Fatiguso, L.M. Galantucci, A proposal for a new standard quantification of damages of cultural heritages, based on 3D scanning, SCIRES-IT-Scientific RESearch and Inform. Technol. 8 (1) (2018) 121–138, <https://doi.org/10.2423/i22394303v8n1p121>.
- [32] R.A. Galantucci, F. Fatiguso, Advanced damage detection techniques in historical buildings using digital photogrammetry and 3D surface analysis, *J. Cult. Herit.* 36 (2019) 51–62, <https://doi.org/10.1016/j.culher.2018.09.014>.
- [33] C. Biscarini, I. Catapano, N. Cavalagli, G. Ludeno, F.A. Pepe, F. Ubertini, UAV photogrammetry, infrared thermography and GPR for enhancing structural and material degradation evaluation of the Roman masonry bridge of Ponte Lucano in Italy, *NDT & E Int.* 115 (2020), 102287, <https://doi.org/10.1016/j.ndteint.2020.102287>.
- [34] P. Forlin, R. Valente, M. Kázmér, Assessing earthquake effects on archaeological sites using photogrammetry and 3D model analysis, *Digit. Appl. Archaeol. Cult. Heritage* 9 (2018), e00073, <https://doi.org/10.1016/j.daach.2018.e00073>.
- [35] A. Ulvi, Using UAV photogrammetric technique for monitoring, change detection, and analysis of archeological excavation sites, *J. Comput. Cult. Heritage (JOCCH)* 15 (3) (2022) 1–19, <https://doi.org/10.1145/3522742>.
- [36] R.A. Galantucci, F. Fatiguso, Advanced damage detection techniques in historical buildings using digital photogrammetry and 3D surface analysis, *J. Cult. Herit.* 36 (2019) 51–62, <https://doi.org/10.1016/j.culher.2018.09.014>.
- [37] S. Zhao, F. Kang, J. Li, C. Ma, Structural health monitoring and inspection of dams based on UAV photogrammetry with image 3D reconstruction, *Autom. Constr.* 130 (2021), 103832, <https://doi.org/10.1016/j.autcon.2021.103832>.
- [38] B. Jafari, A. Khaloo, D. Lattanzi, Deformation tracking in 3D point clouds via statistical sampling of direct cloud-to-cloud distances, *J. Nondestruct. Eval.* 36 (4) (2017) 1–10, <https://doi.org/10.1007/s10921-017-0444-2>.
- [39] X. Kong, Identifying geomorphological changes of coastal cliffs through point cloud registration from UAV images, *Remote Sens.* 13 (16) (2021) 3152, <https://doi.org/10.3390/rs13163152>.
- [40] A. Thelen, X. Zhang, O. Fink, Y. Lu, S. Ghosh, B.D. Youn, Z. Hu, A comprehensive review of digital twin—part 1: modeling and twinning enabling technologies, *Struct. Multidiscip. Optim.* 65 (12) (2022) 1–55, <https://doi.org/10.1007/s00158-022-03425-4>.
- [41] M. Grieves, J. Vickers, Digital twin: Mitigating unpredictable, undesirable emergent behavior in complex systems, in: *Transdisciplinary Perspectives on Complex Systems*, Springer, Cham, 2017, pp. 85–113, [https://doi.org/10.1007/978-3-319-38756-7\\_4](https://doi.org/10.1007/978-3-319-38756-7_4).
- [42] M. Grieves, Digital twin: manufacturing excellence through virtual factory replication, White Paper 1 (2014) (2014) 1–7. [https://www.researchgate.net/publication/275211047\\_Digital\\_Twin\\_Manufacturing\\_Excellence\\_through\\_Virtual\\_Factory\\_Replication](https://www.researchgate.net/publication/275211047_Digital_Twin_Manufacturing_Excellence_through_Virtual_Factory_Replication) (date of last access: 02/18/2023).
- [43] F. Tao, H. Zhang, A. Liu, A.Y. Nee, Digital twin in industry: state-of-the-art, *IEEE Trans. Indu. Inform.* 15 (4) (2018) 2405–2415, <https://doi.org/10.1109/TII.2018.2873186>.
- [44] F. Tao, M. Zhang, Digital twin shop-floor: a new shop-floor paradigm towards smart manufacturing, *IEEE Access* 5 (2017) 20418–20427, <https://doi.org/10.1109/ACCESS.2017.2756069>.
- [45] F. Jiang, L. Ma, T. Brody, K. Chen, Digital twin and its implementations in the civil engineering sector, *Autom. Constr.* 130 (2021), 103838, <https://doi.org/10.1016/j.autcon.2021.103838>.
- [46] M. Mohammadi, M. Rashidi, V. Mousavi, A. Karami, Y. Yu, B. Samali, Quality evaluation of digital twins generated based on UAV photogrammetry and TLS: bridge case study, *Remote Sens.* 13 (17) (2021) 3499, <https://doi.org/10.3390/rs13173499>.
- [47] A. Marra, S. Gerbino, A. Greco, G. Fabbrocino, Combining integrated informative systems and historical digital twin for maintenance and preservation of artistic assets, *Sensors* 21 (17) (2021) 5956, <https://doi.org/10.3390/s21175956>.
- [48] M. Falcone, A. Origlia, M. Campi, S. Di Martino, From architectural survey to continuous monitoring: graph-based data management for cultural heritage conservation with digital twins, *Int. Arch. Photogramm., Remote Sens. Spatial Inf. Sci.* 43 (2021) 47–53, <https://doi.org/10.5194/isprs-archives-XLIII-B4-2021-47-2021>.
- [49] K. Themistocleous, E. Evagorou, C. Mettas, D. Hadjimitsis, The use of digital twin models to document cultural heritage monuments, in: *Earth Resources and Environmental Remote Sensing/GIS Applications XIII* 12268, SPIE, 2022, October, pp. 55–64, <https://doi.org/10.1117/12.2636332>.
- [50] M. Pregnolato, S. Gunner, E. Voyagaki, R. De Risi, N. Carhart, G. Gavriel, C. Taylor, Towards civil engineering 4.0: concept, workflow and application of digital twins for existing infrastructure, *Autom. Constr.* 141 (2022), 104421, <https://doi.org/10.1016/j.autcon.2022.104421>.
- [51] AgiSoft Metashape Professional (Version 1.6.2) (Software), Retrieved from, <http://www.agisoft.com/downloads/installer/>, 2020. date of last access: 02/18/2023.
- [52] S. Ullman, The interpretation of structure from motion, *Proc. Royal Soc. of London. Series B. Biol. Sci.* 203 (1153) (1979) 405–426, <https://doi.org/10.1098/rspb.1979.0006>.
- [53] A.M. Andrew, Multiple view geometry in computer vision, *Kybernetes* 30 (9/10) (2001) 1333–1341, [https://doi.org/10.1108/k.2001.30.9\\_10.1333.2](https://doi.org/10.1108/k.2001.30.9_10.1333.2).
- [54] K. Kingsland, Comparative analysis of digital photogrammetry software for cultural heritage, *Digit. Appl. Archaeol. Cult. Heritage* 18 (2020), e00157, <https://doi.org/10.1016/j.daach.2020.e00157>.
- [55] I. Alcardi, F. Chiabrando, A.M. Lingua, F. Noardo, Recent trends in cultural heritage 3D survey: the photogrammetric computer vision approach, *J. Cult. Herit.* 32 (2018) 257–266, <https://doi.org/10.1016/j.culher.2017.11.006>.

- [56] Y. Chen, G. Medioni, Object modelling by registration of multiple range images, *Image Vis. Comput.* 10 (3) (1992) 145–155, [https://doi.org/10.1016/0262-8856\(92\)90066-C](https://doi.org/10.1016/0262-8856(92)90066-C).
- [57] P.J. Besl, N.D. McKay, Method for registration of 3-D shapes, in: *Sensor Fusion IV: Control Paradigms and Data Structures* 1611, SPIE, 1992, April, pp. 586–606, <https://doi.org/10.1117/12.57955>.
- [58] D.P. Huttenlocher, G.A. Klanderman, W.J. Rucklidge, Comparing images using the Hausdorff distance, *IEEE Trans. Pattern Anal. Mach. Intell.* 15 (9) (1993) 850–863, <https://doi.org/10.1109/34.232073>.
- [59] D. Lague, N. Brodu, J. Leroux, Accurate 3D comparison of complex topography with terrestrial laser scanner: application to the Rangitikei canyon (NZ), *ISPRS J. Photogramm. Remote Sens.* 82 (2013) 10–26, <https://doi.org/10.1016/j.isprsjprs.2013.04.009>.
- [60] W. Graves, K. Aminfar, D. Lattanzi, Full-scale highway bridge deformation tracking via photogrammetry and remote sensing, *Remote Sens.* 14 (12) (2022) 2767, <https://doi.org/10.3390/rs14122767>.
- [61] Database for National Register of Historic Places, National Park Service, Retrieved from: <https://www.nps.gov/subjects/nationalregister/database-research.htm>, 2020, date of last access: 02/18/2023.
- [62] Onozawa, Final Historical Structures Report Taleyfak Spanish Bridge, Tollai Talaifak, Agat, Guam, Available online: <https://www.pacificpreservation.org/plans>, 2008, date of last access: 02/18/2023.
- [63] Dominic J. Lizama, Colonization to Construction: Bridging the Gap Between Ancient Chamorro, Spanish Colonial & Modern Architecture on Guam, Undergraduate Honors Theses. 9, <https://repository.usfca.edu/honors/9>, 2016, date of last access: 02/18/2023.
- [64] Nomination form for Taleyfac Bridge submitted to National Register of Historic Places in the US, Retrieved from, <https://npgallery.nps.gov/GetAsset/c508c22a-b58b-4380-a27e-6c7580b04d93>, 1974, date of last access: 02/18/2023.
- [65] CloudCompare (version 2.10.2) [GPL Software], Available online: <http://www.cloudcompare.org/>, 2020, date of last access: 02/18/2023.
- [66] M.W. Smith, J.L. Carrivick, D.J. Quincey, Structure from motion photogrammetry in physical geography, *Prog. Phys. Geogr.* 40 (2) (2016) 247–275, <https://doi.org/10.1177/03091331561580>.
- [67] Kristopher Campbell, Nicola Ann Stevens, Myra Lydon, Thomas Neeson, Su Taylor, Alan O'Connor, A Review of the Data Held on 3,437 Masonry Arch Bridges in Northern Ireland, *Civil Engineering Research in Ireland*, 2020, p. 3, <https://sword.cit.ie/ceri/2020/3/3>, date of last access: 02/18/2023.
- [68] Q. Han, J. Xu, A. Carpinteri, G. Lacidogna, Localization of acoustic emission sources in structural health monitoring of masonry bridge, *Struct. Control. Health Monit.* 22 (2) (2015) 314–329, <https://doi.org/10.1002/stc.1675>.
- [69] N. Grillanda, G. Milani, S. Ghosh, B. Halani, M. Varma, SHM of a severely cracked masonry arch bridge in India: experimental campaign and adaptive NURBS limit analysis numerical investigation, *Constr. Build. Mater.* 280 (2021), 122490, <https://doi.org/10.1016/j.conbuildmat.2021.122490>.
- [70] L. Cheng, S. Chen, X. Liu, H. Xu, Y. Wu, M. Li, Y. Chen, Registration of laser scanning point clouds: a review, *Sensors* 18 (5) (2018) 1641, <https://doi.org/10.3390/s18051641>.
- [71] T. Kaiser, C. Clemen, H.G. Maas, Automatic co-registration of photogrammetric point clouds with digital building models, *Autom. Constr.* 134 (2022), 104098, <https://doi.org/10.1016/j.autcon.2021.104098>.